JOURNAL OF GEOPHYSICAL RESEARCH, VOL. 113, F03012, doi:10.1029/2007JF000896, 2008

Quantifying the morphology and growth of levees in aggrading submarine channels

Kyle M. Straub[1,2] and David Mohrig[3]

Received 18 August 2007; revised 26 March 2008; accepted 28 May 2008; published 2 August 2008.

[1] Levees are the primary elements of self-formed submarine channels, yet little is know about their morphodynamics. We present field observations of static levee morphology and stratigraphy in addition to laboratory experiments that link levee morphodynamics to turbidity current flow properties. These observations are used to motivate a levee growth model. Using a three-dimensional seismic volume, we mapped the depositional patterns associated with a network of submarine channels defined by prominent levees on the continental slope offshore Brunei. Levee taper increases rapidly as channel depth increases from 5 to 50 m and then increases at an ever diminishing rate for channels between 50 and 72 m of depth. A similar relationship between levee taper and channel relief was observed in a set of laboratory experiments. We released turbidity currents into a straight channel positioned within a larger experimental basin. The currents were able to interact with the overbank environment and therefore construct channel bounding levees. We link periods of rapid change in levee growth in our experiments to the vertical structure of suspended sediment in turbidity currents. Our field and laboratory observations suggest that the most important parameters controlling levee morphodynamics are the degree of channel confinement and the vertical structure of suspended-sediment concentration profiles. Our levee growth model couples a simple advection settling model for currents with a vertical sediment concentration profile defined by the Rouse equation. The model reproduces our field and laboratory observations of levee growth and provide a method to estimate current thickness from levee stratigraphy.

Citation: Straub, K. M., and D. Mohrig (2008), Quantifying the morphology and growth of levees in aggrading submarine channels, *J. Geophys. Res.*, *113*, F03012, doi:10.1029/2007JF000896.

1. Introduction

[2] Mapping of continental margins has revealed surfaces covered by numerous submarine channel systems [*Damuth et al.*, 1983; *Pirmez and Flood*, 1995; *Posamentier and Kolla*, 2003]. These channels are the dominant conduits for transport of terrigenous sediment into the deep sea and impart a first-order control on continental-slope topography [*Kostic et al.*, 2002; *Pirmez et al.*, 2000]. Submarine channels are bounded over much of their length by prominent natural levees. These levees are built from the overspill and deposition of sediment contained in turbidity currents [*Dennielou et al.*, 2006; *Hay*, 1987; *Pirmez et al.*, 1997; *Skene et al.*, 2002; *Straub et al.*, 2008]. In net aggradational settings, levees are the primary elements of self-formed channels and their deposits provide a cumulative record of channel history compared to deposits located in channel thalwegs where frequent episodes of local erosion can produce complicated stratigraphic histories. For self-formed channels the temporal and spatial growth of levees sets channel relief or depth. This relief in turn influences the degree to which turbidity currents are able to spill out of the confining channels and construct the regional overbank surface. Unfortunately, the wealth of geometric data defining the levees of submarine channels is not matched by an equivalent set of data defining the levee-building processes. Measurements of out-of-channel flow are less common than the small set of direct observations from turbidity currents confined to submarine channels themselves [*Hay*, 1987; *Khripounoff et al.*, 2003; *Xu et al.*, 2004].

[3] Measurements from natural systems and laboratory experiments document numerous cases in which depositional submarine channels aggrade distances equal to or exceeding multiple channel depths while undergoing almost no change in channel planform shape and position [*Deptuck et al.*, 2003; *Posamentier*, 2003; K. M. Straub and D. Mohrig, Constructional canyons built by sheet-like turbidity currents: Observations from offshore Brunei Darussalam, submitted to *Journal of Sedimentary Research*, 2008]. This

[1]Department of Earth, Atmosphere, and Planetary Sciences, Massachusetts Institute of Technology, Cambridge, Massachusetts, USA.
[2]Now at Department of Geology and Geophysics, University of Minnesota, Minneapolis, Minnesota, USA.
[3]Department of Geological Sciences, University of Texas at Austin, Austin, Texas, USA.

0148-0227/08/2007JF000896$09.00

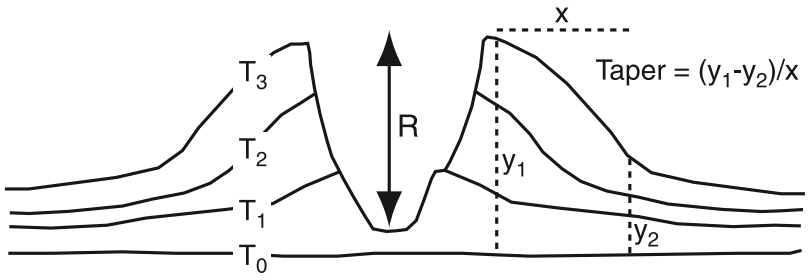

Figure 1. Definition sketch for the geometry of a levee.

nearly vertical climb of channel form in space requires rates of overbank sedimentation that are nearly equivalent to the in-channel deposition rates. Several processes have been identified that can transfer some fraction of a channelized turbidity current onto the regional overbank surface, including flow splitting and flow spilling [*Clark and Pickering*, 1996; *Piper and Normark*, 1983; *Straub et al.*, 2008]. A portion of the sediment contained in these overbanking flows is deposited on and incorporated into the channel-bounding levees. Several authors have proposed that submarine levee architecture is controlled by 4 properties of the overbanking flow: (1) current height, H; (2) current velocity, U; (3) diameter and size distribution of suspended particles; and (4) structure of the suspended-sediment concentration profile [*Pirmez and Imran*, 2003; *Skene et al.*, 2002; *Straub et al.*, 2008]. In this paper we focus on the control of these 4 properties as they relate to the evolution of the channel-levee taper. Levee taper is defined here as the change in deposit thickness over some specified distance measured at a right angle to the local direction of the channel centerline (Figure 1). Levee taper is equal to the levee surface slope in the special case where the bank of the original channel form was both perfectly flat and horizontal. In our analysis we focus on changes in the taper of the bulk levee as a function of relief. The bulk levee is defined as a package of sediment deposited on a relatively flat surface with basal sediments deposited coevally with initiation of channel construction. The bulk levee is constructed through deposition of individual sediment beds, each having their own bed taper. It is worth noting that if a levee is constructed by deposition of sediment layers, where each layer has identical tapers, the bulk levee taper will systematically increase with deposit thickness in a linear trend. Deviations away from a linear trend on a plot of bulk levee taper versus bulk levee thickness, therefore, point to changes in taper of the individual sediment beds that comprise the bulk levee. We analyze how taper changes during cases where levee growth is associated with both channel deepening and channel filling and relate these changes to properties of the channel-constructing turbidity currents. A better resolved understanding of levee morphodynamics will aid numerical formulations of seascape evolution that incorporate submarine channel processes.

[4] Submarine levees have been the subject of several quantitative studies during the past ten years [*Pirmez and Flood*, 1995; *Pirmez et al.*, 1997; *Pirmez and Imran*, 2003; *Skene et al.*, 2002]. *Pirmez et al.* [1997] and *Pirmez and Imran* [2003] focused on the temporal and spatial fining of particles composing levee deposits as a channel deepened. This change in deposit particle size was related to the progressive confinement of currents within the banks of the channel itself. These studies did not relate vertical trends in levee grain size to the evolution of levee morphology. *Skene et al.* [2002] studied the morphology of submarine levees by comparing characteristics of levee thickness from 6 different channel systems from around the world. This study developed methods for measuring the spatial decay rate of levee thickness in both the flow direction parallel to the channel centerline and in cross sections oriented perpendicular to the primary transport direction. *Skene et al.* [2002] calculated these spatial decay rates for only the total levee deposit, making no attempt to analyze how these parameters might have varied as channels either deepened or filled. We aim here to develop a joint description of how levee deposit particle size and morphology coevolve in response to changes in channel relief.

[5] Submarine levees share many characteristics with terrestrial levees that develop on river banks. Levee height and width are proportional to channel depth in both environments [*Adams et al.*, 2004; *Cazanacli and Smith*, 1998] and levee slope is influenced by the depth, velocity and particle sizes contained in overbanking flows [*Filgueira-Rivera et al.*, 2007; *Pizzuto*, 1987]. Even though it is easy to access terrestrial levees, the processes controlling levee development in this environment are not correspondingly well resolved. The small surface slopes and tapers associated with terrestrial levees make it difficult to resolve differences in these properties [*Brierley et al.*, 1997; *Rowland et al.*, 2005]. In addition, relatively little subsurface data has been collected over active or abandoned terrestrial channels, placing limits on the ability to study the temporal evolution of levee morphologies. Submarine levees on channels of comparable size are typically thicker, wider, and have larger tapers than those associated with rivers [*Pirmez*, 1994]. These differences in levee properties are thought to be a consequence of the difference in density of the ambient fluid present in the two environments: ocean water is roughly 800 times denser than air and the ocean water is almost as dense as the sediment-transporting turbidity currents themselves. This small density contrast helps to promote turbidity-current heights that can be much greater than the relief of their guiding channels [*Mohrig and Buttles*, 2007], allowing for the continuous overspill of current and sediment onto the marine overbank surface [*Clark and Pickering*, 1996]. It is our hope that an improved understanding of levee formation and growth in the submarine environment will also aid our quantitative and conceptual understanding of terrestrial levee dynamics and add to a general evolution model for self-formed channels.

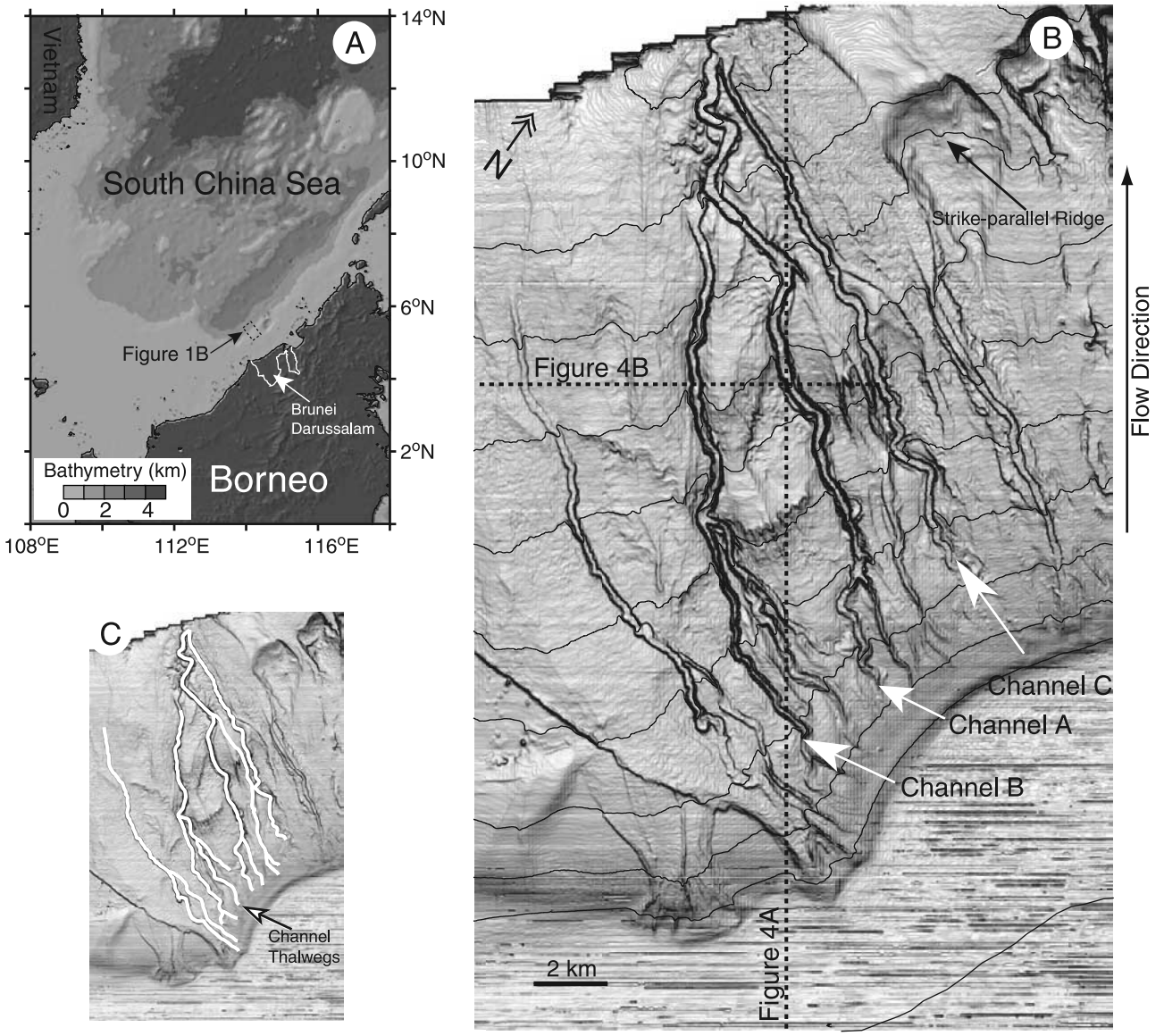

Figure 2. Maps of South China Sea and the study region. (a) Regional bathymetry map for the South China Sea with location of study region offshore Brunei defined by dashed box. (b) Slope map of study region highlighting the network of leveed submarine channels. This and other slope maps presented here were created by calculating the average absolute value for the local surface slope based on the surface elevations at each data bin and its eight immediate neighbors. High values of surface slope defining channel walls and detachment scarps have high gray-scale intensities (appear dark colored). Contour lines defining 100 m bathymetric intervals are superimposed on the dip map. Locations for seismic sections in Figure 4 are represented by dashed lines. Arrows and labels identify channels A, B, and C.

[6] This paper links measurements of submarine levees and stratigraphy from a continental slope setting with data from laboratory experiments. Taken together these measurements motivate the development of a simple, quantitative sedimentation model that is intended to illuminate the basic morphodynamics of submarine levee growth. We begin by analyzing the depositional patterns associated with a tributary system of submarine channels on the continental margin offshore Borneo. Using an industry-grade 3D seismic volume we quantify how levee taper varies as a function of channel relief. Observations from offshore Borneo motivate a laboratory study where we document the influence of the suspended sediment concentration profile and degree of current confinement by levee growth on the evolution of levee morphology, specifically deposition rate and levee taper. We then develop a levee-growth model based on a coupling of an advection-settling model to a suspended sediment concentration profile defined by the Rouse equation. This model is then tested against data from offshore Borneo. Finally, we use this model to estimate channel forming flow thicknesses.

2. Continental Margin Offshore Borneo

[7] The present-day continental slope offshore northern Borneo (Figure 2) has been a passive margin since the late

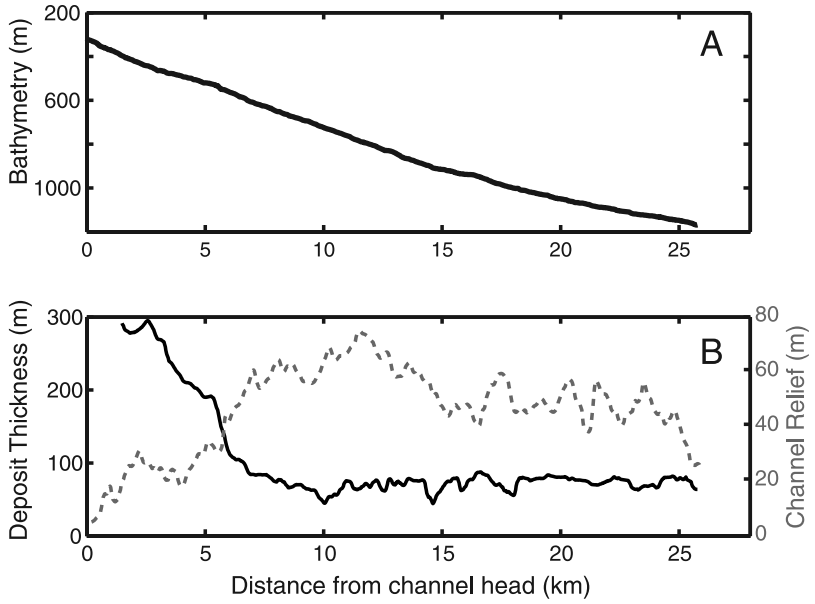

Figure 3. Downstream trends for Channel A thalweg. (a) Profile of channel thalweg bathymetry following channel centerline as a function of distance from channel head. (b) Channel relief and in-channel sediment thickness measured for interval between seafloor and mapped detachment surface as a function of distance from channel head.

Miocene [*Hiscott et al.*, 1997; *Hutchison*, 2004]. The morphology of this continental margin is greatly influenced by sediment delivered from the Baram, Belait, and Tutong rivers [*Hiscott*, 2001; *Hutchison*, 2004]. These three rivers are also responsible for building the Baram-Champion delta complex and construction of a continental shelf that is 50–70 km wide and underlain by 8–9 km of post-Eocene siliclastic sediments [*Sandal*, 1996]. These sediments are derived from uplifted rocks of the Rajang-Crocker ranges in central Borneo. Erosion rates measured in these ranges are among the highest in the world and have resulted in high sediment-discharge rates to the South China Sea since the Eocene [*Hutchison*, 2004; *Sandal*, 1996].

[8] In the study area the continental shelf-slope break occurs at a water depth of ~200 m (Figure 2b). The seabed then descends for the next roughly 60 km until reaching the floor of the Borneo Trough at a water depth of 2800 m. The upper slope is characterized by a relatively steep average gradient of 3.2°. Superimposed on this regional dipping surface are several tributary networks of submarine channels and a series of strike-parallel ridges. These ridges are the product of diaperism by mobile overpressured shale [*Demyttenaere et al.*, 2000; *Ingram et al.*, 2004; *van Rensbergen et al.*, 1999]. The combination of the high surface gradient and shale diapirism has lead to multiple mass-failure events on the upper slope. Several head scarps documenting the release points for these large detachments are still visible on bathymetric maps of the present-day seafloor (Figure 2b).

2.1. Seismic Data Set Parameters

[9] Our study of leveed submarine channels takes advantage of a 4000 km^2 industry-grade 3-D seismic volume covering the continental slope offshore Brunei Darussalam. The specific area is a tributary network of channels that covers 555 km^2 of this larger survey (Figure 2b). We focused on the shallow sedimentary section positioned between the seafloor and a subsurface depth defined acoustically by an additional 0.3 s of two-way traveltime. The frequency roll-off for this portion of the seismic volume is near 80 Hz, providing a vertical resolution for buried deposits of $\leq$3 m. The entire survey was collected on a horizontal grid with 25 $\times$ 25 m^2 spacing. The seismic reflectors defining the seafloor and a significant subsurface horizon were picked manually on every grid inline in order to produce the highest-quality set of digital elevation models for our study area.

2.2. Network of Leveed Channels

[10] We focus on a relatively small channel network with a catchment that is approximately 6 $\times$ 24 km in the strike and dip directions (Figure 2b). Even though this network is located directly downslope from the Champion shelf-edge delta, none of its channels can be directly traced to the terrestrial system. All submarine channels of detectable size initiate at positions 1–2 km downslope of the shelf break. These most proximal channels are presently situated approximately 250 m below mean sea level. The distal end to the network is at 1200 m below mean sea level. Channels possess a consistent pattern of growth. Channel relief or depth systematically increases from 0 m to an average value of 40 m over approximately the first 7 km downslope of the shelf edge. Following this zone of consistent growth, the three largest channels in the network approach a constant relief for the remainder of their lengths. The long profile for Channel A (Figure 2b) and the corresponding variation in channel relief or depth is presented in Figure 3. Subsurface imaging shows that channel relief is entirely the product of levee construction (Figure 4). Seismic cross sections oriented perpendicular to channels reveal higher-amplitude reflectors in channel thalwegs compared to overbank surfaces, suggesting that channel deposits are coarser grained

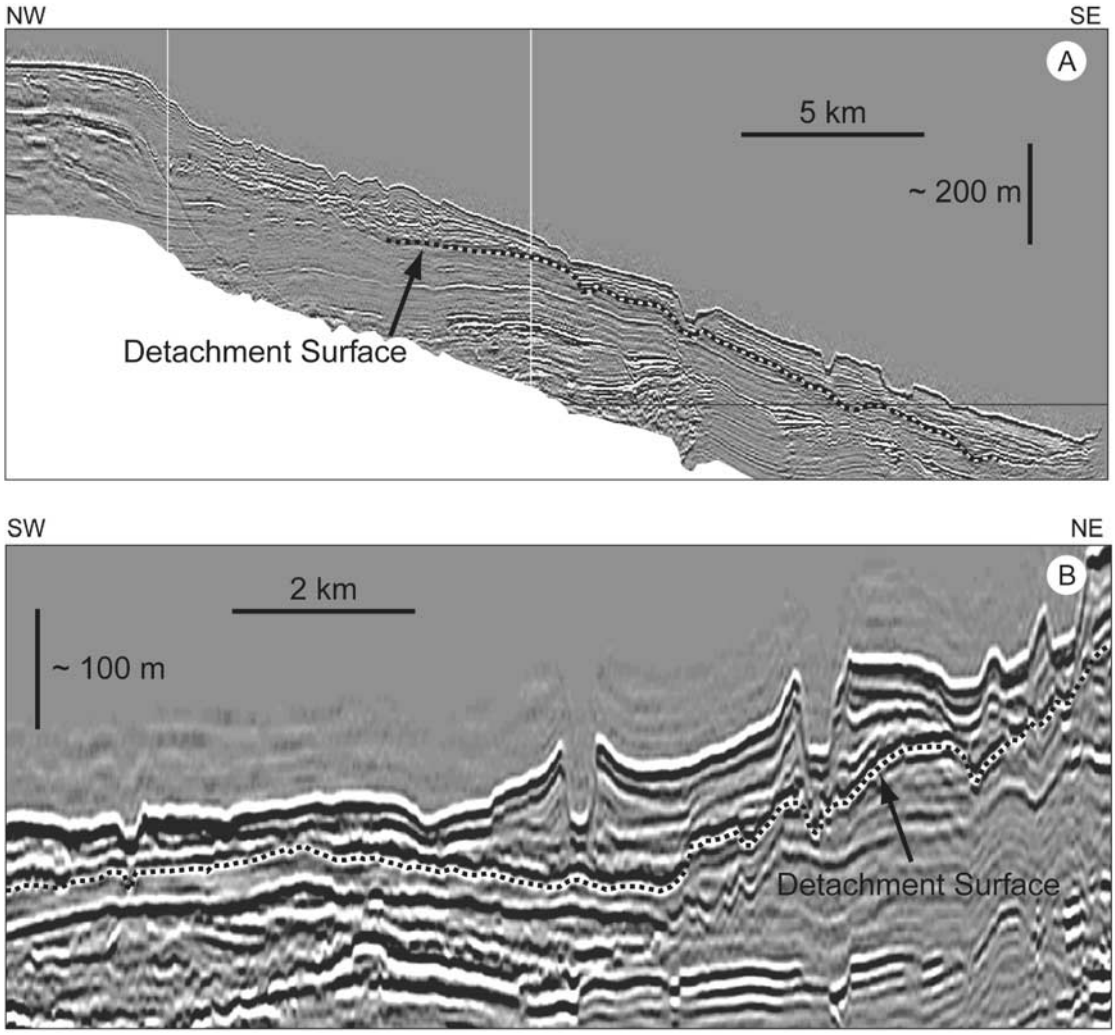

Figure 4. Characteristic dip- and strike-oriented seismic lines for study region showing a portion of the regional stratigraphy from the seafloor to below the area of interest in this study. Dashed lines follow subsurface detachment horizon created by mass-failure release which reset margin to an unchannelized state. (a) Characteristic dip section spanning upper continental slope from present-day continental shelf to 1200 m of water depth. (b) Characteristic strike section. Section intersects two prominent channels at close to perpendicular angles to channel centerlines. Velocity increases with depth so vertical scale is an approximate vertical average for the section.

than levee and regional overbank deposits [*Prather et al.*, 1998].

2.3. Pattern of Sediment Deposition Within Channel Network

[11] Producing a map of sediment deposition associated with the leveed channels requires the regional mapping of two surfaces, the seafloor and some prominent horizon in the shallow subsurface. Using the 3-D seismic volume we have mapped a shallow (<0.25 s TWT below seafloor) regional surface beneath the network of interest. We chose to map the shallow subsurface reflector marked in Figure 4 because it possesses consistently strong reflection amplitude that allowed us to track the horizon beneath the majority of the network area. Inspection of a map of this surface (Figure 5) reveals a dearth of local topography associated with paleochannels, as well as a laterally persistent detachment scarp and slide plane associated with a regionally extensive, mass-failure event (>40 km^2). The detachment scarp preserves 30–50 m of relief suggesting a mass failure of comparable thickness. Downslope of the scarp are several long linear striations which were likely formed as the mass failure moved across the slide plain (Figure 5). The seismically defined stratigraphy indicates that the network area has been the site of persistent sediment deposition since the release of the youngest mass failure. Development of the leveed channels on top of the regional extensive and relatively smooth slide plane provides us with the simplest possible initial condition for studying the evolution of aggradational submarine channels and levee taper.

[12] A map of sediment deposition associated with the channel network was created by differencing the seafloor and subsurface horizons. This map was converted from two-way traveltime to deposit thickness using a seismic velocity of 1700 m/s, the measured average velocity for the first 300 m of sediment at the nearest point of well control,

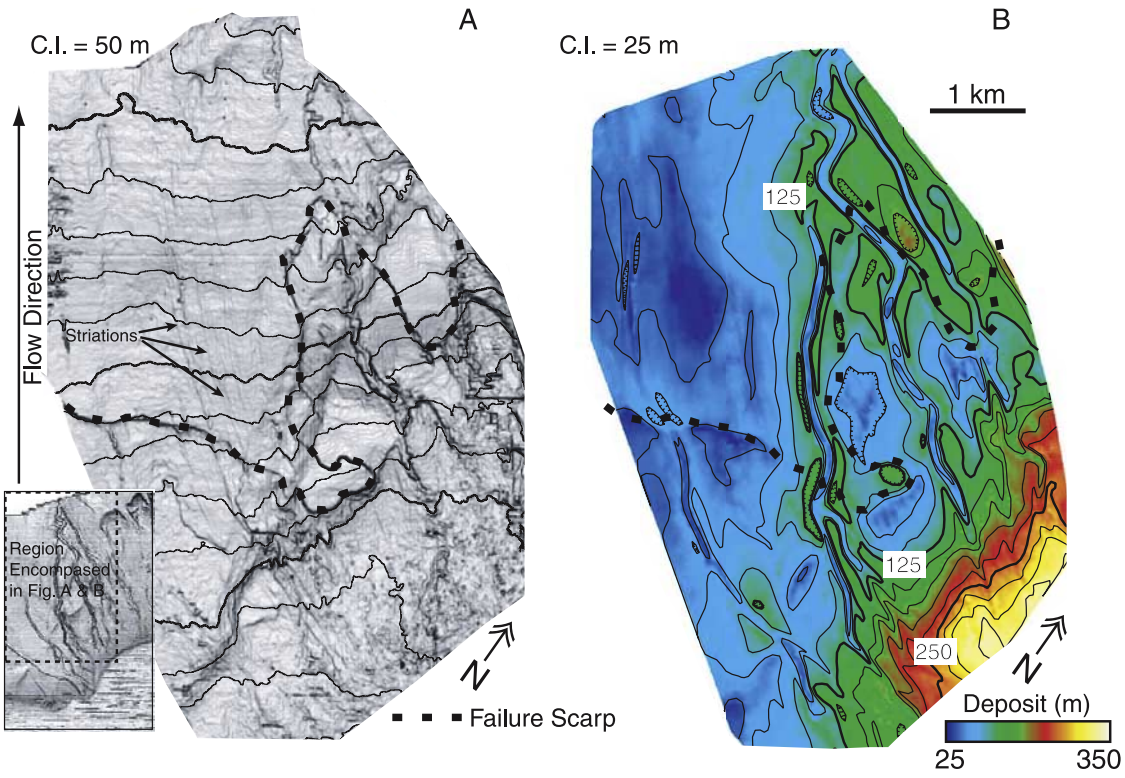

Figure 5. Maps of mapped subsurface seismic horizon and deposit thickness measured between seafloor and subsurface horizon. Dashed lines mark location of failure scarp. Insert delineates boundaries of two maps. (a) Slope map of regionally mapped subsurface horizon. Horizon defines scarp and slide plane associated with release of mass failure. Contours define depth below present-day sea level. Contour interval is 50 m. (b) Deposit thickness measured between seafloor and regionally mapped subsurface horizon. Contour interval is 25 m.

60 km to the southwest of our study area [*van Rensbergen et al.*, 1999]. Several observations can be made from this map of recent deposition (Figure 5b). First, the primary control on interval thickness is simply distance from the shelf edge, with sedimentation decreasing in the downslope direction. This depositional pattern is consistent with this region of Borneo margin undergoing progradation. In addition to this regional trend, the observed pattern of sedimentation is locally influenced by the high surface gradients associated with the most recent detachment scarp. Local minima in sediment deposition are positioned directly up-slope of the scarp while depositional thicks are located directly downslope of the scarp (Figure 5b). Finally, thick levee deposits define the margins of every channel and indicate that this tributary network grew under net depositional conditions. In-channel deposition appears anticorrelated to local channel relief or depth (Figure 3b). Sediment deposition on the beds of channels decreases rapidly over the same locations that channel depth is observed to rapidly increase. Both thalweg deposition and channel relief achieve approximately constant values at approximately the same downslope position (Figure 3b). Biostratigraphic control assembled from subsurface samples collected at petroleum exploration wells located roughly 60 km to the southwest of our study area strongly suggest that all of this sedimentation is of Quaternary age [*Hiscott*, 2001]. Further refinement of the age for the studied depositional network will require coring within the study area itself.

2.4. Quantifying Overbank Deposition and Levee Growth

[13] The map of deposit thickness throughout the submarine channel network contains the spatial information that defines levee form and sediment accumulation on the distal overbank surface. To characterize this depositional pattern we have performed the following analysis. First, we identified the location of every grid node on the thickness map that corresponds to a channel thalweg (Figure 2c) With this network in place we calculated the path length to the nearest channel thalweg for every grid node on the map. This allowed us to examine every local measure of thickness as a function of distance from the closest channel thalweg. We then sorted and assembled all of the data points using this distance. The binning width was 25 m, the horizontal spacing associated with the 3-D seismic cube itself. Collapsing the data onto a single trendline allows us to capture both the mean depositional signal as well as the magnitude of variability about this trend associated with local topographic effects. Mean thickness and coefficient of variation, CV, defining both levee and background overbank deposition are presented in Figure 6.

[14] The plot of average sediment thickness versus distance from a channel center allows us to define and

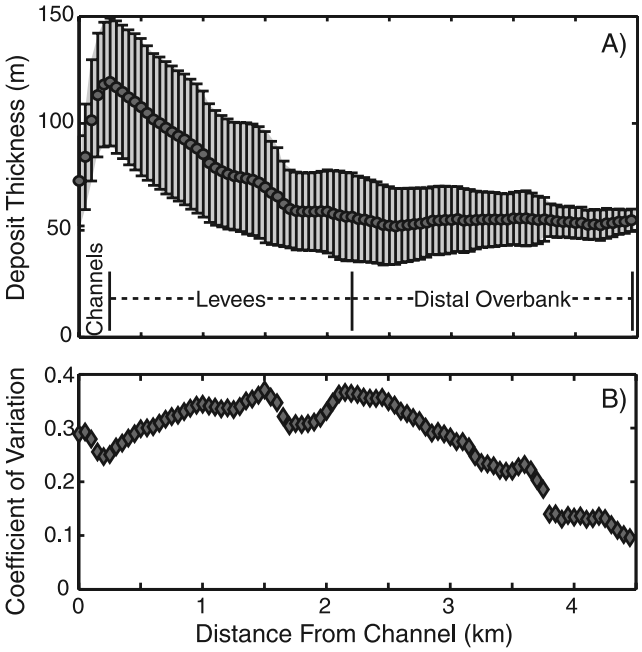

Figure 6. Change in deposit thickness as a function of shortest distance to a channel thalweg. (a) Mean thickness of deposit measured in bins spaced every 25 m from closest channel thalweg. Error bars represent ±1 standard deviation of data in each bin. (b) Coefficient of variation for deposit thickness sample bins.

characterize three depositional zones within the network. The first zone makes up the channels themselves. Average channel half width is 125 m and over this distance deposit thickness increases from 65 m at the thalweg to 122 m at the levee crest (Figure 6a). The second zone defines the average levee form and runs between 125 m to 2200 m from a channel centerline. Over this lateral distance, sediment thickness drops from 122 m at the levee crest to 55 m its distal termination. It is not obvious where to place the distal end of the levee on the basis of mean thickness only. We have refined the location by taking advantage of the spatial structure in the coefficient of variation for deposit thickness. Coefficient of variation maintains an approximately constant, relatively large value for a distance up to 2200 m from a channel center. After this point values for CV systematically decrease with increasing separation from a channel. We take the transition from a roughly constant CV to a continuously decreasing one as defining the boundary between the levee and background overbank surface. We expect a greater variation in depositional thickness to be associated with focused levee deposition versus the background sedimentation building the regional overbank surface. Sedimentation on the distal overbank has produced a deposit with a nearly constant thickness of 55 m.

[15] Analysis of the three depositional zones reveals two system properties that are particularly relevant to inferring behavior of the evolving network. First, sedimentation in channel thalwegs is only somewhat greater than the background deposition associated with the far-field overbank surface, 65 m versus 55 m, respectively. These nearly equal amounts of in-channel versus overbank deposition points to development of channels that are laterally stable and not prone to avulsion. Second, the characteristic width of the total levee package is 8.4 times the average channel width (Figure 6a). As most channels in our study network are separated by less than 2 km from their closest neighboring channel, this levee distance suggests that some fraction of overbanking flow from currents moving down one channel is likely to reenter an inactive or neighboring channel and continue to move downslope.

[16] Next we sought to unravel how levee morphology, specifically taper, evolved as channel relief increased. The vertical resolution associated with subsurface sediment bodies was not high enough to resolve this trend by measuring a succession of stacked levee deposits in seismic cross section (Figure 4). Because of this we regrouped the regional thickness data summarized in Figure 6a by relief of the nearest channel. By doing this we created a series of profiles defining deposit thickness as a function of distance from the nearest channel thalweg for 5-m increments of channel relief. Levee taper was measured from each of these profiles by measuring the change in total levee deposit thickness over a lateral distance equal to two channel widths. Previous studies have characterized levee slope or taper using spatial decay rates calculated by fitting exponential curves to the profiles [*Pizzuto*, 1987; *Skene et al.*, 2002]. *Skene et al.* [2002] compared exponential and linear models which describe the decrease in levee thickness with distance away from a channel thalweg and found no statistically meaningful difference between the two models. Levee taper was found to systematically increase from 0.008 m/m to 0.041 m/m as channel relief or depth increased from 5 to 25 m. This increase in taper was not constant. Levee taper increased at an ever diminishing rate, with channel segments up to 72 m deep having a levee taper of only 0.056 m/m (Figure 7). This pattern of rapid increase

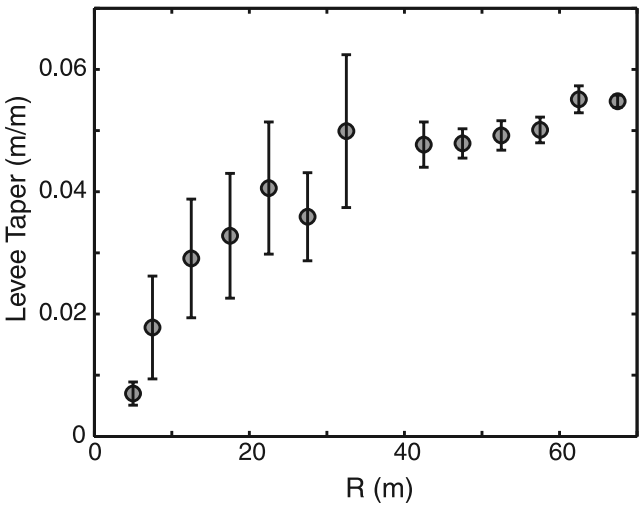

Figure 7. Change in the levee-deposit taper as a function of channel relief. Levee taper was defined from linear regression best fit lines through plots of average cumulative deposit thickness versus distance from channel. Taper was measured over a distance equivalent to two channel widths for each value of channel relief. Error bars are ±1 standard deviation measured from variability in data defining deposit thickness versus distance from channel plots for each bin of channel relief.

in levee taper when channel relief is small followed by slower increases in taper for higher-relief channels suggests a change in sedimentation properties for overbanking flow as the turbidity currents became relatively more confined within channels. In the following sections we use laboratory experiments and a numerical model to investigate the dynamics of levee growth and the influence of current properties in the evolution of levee taper as a function of channel relief.

3. Laboratory Experiments

[17] Turbidity currents and their depositional and erosional patterns have been studied at laboratory scale for over 4 decades [*Keevil et al.*, 2006; *Middleton*, 1966; *Parker et al.*, 1987; *Straub et al.*, 2008]. The vast majority of these experiments have been conducted in flumes specifically designed to suppress across-flow variation in the flow field [*Felix et al.*, 2005; *Hallworth et al.*, 1993; *Parker et al.*, 1987]. These studies refined our understanding of the stream-wise evolution of two-dimensional turbidity currents. In recent years, several studies have examined depositional and erosional patterns associated with channel formation and growth [*Mohrig and Buttles*, 2007; *Straub et al.*, 2008; *Yu et al.*, 2006]. We present laboratory results that focus on resolving at a reduced scale the growth of channel bounding levees. In particular, we monitor the depositional patterns, specifically deposit thickness, composition (grain size), and levee taper, resulting from the continuous overspill of an upper fraction of a turbidity current in a straight channel. Deposit properties resulting from this experiment were summarized by *Mohrig et al.* [2005] but were not systematically related to the stream-wise velocity and suspended-sediment concentration profiles for the levee-building turbidity currents. We relate deposit properties to the following current properties: (1) fraction of total current thickness located above the rim of the channel-confining levees, (2) vertical profiles of suspended sediment concentration, and (3) stream-wise velocity profile. The overarching aim of this experiment was to collect data relevant to the morphodynamics of levee growth that is missing in the static morphology and stratigraphy of natural settings such as offshore Brunei.

3.1. Experimental Setup

[18] Nine sediment-laden currents were released into a basin that is 5 m long, 5 m wide, and 1.2 m deep that remained filled with water throughout the experiment (Figure 8). Before filling the basin with fresh water, a channel was constructed on its floor. The channel had a length of 3 m, had an initial relief of 50 mm, 30° channel sidewalls and maximum and minimum channel widths of 0.77 and 0.6 m respectively (Figure 9a). The initial channel was constructed from six 0.5-m-long concrete forms placed flush end to end. The channel had no initial downstream bed slope. After traversing the 3.0-m-long channel, each current spread out onto a short unconfined surface before plunging into a moat where it was removed from the basin via perforated pipes, thereby preventing current reflections off of the tank sidewalls.

[19] All turbidity currents were composed of the same mixture of clear water and suspended sediment. This mixture produced currents that entered the channel with a bulk density of 1024 kg/m^3. Crushed silica was used as sediment and had a cumulative grain size distribution characterized by a D1, D5, D16, D50, D84, D95, and D99 equal to nominal diameters of 1.4 μm, 2.4 μm, 6 μm, 29 μm, 59 μm, 89 μm, and 133 μm, respectively. The mixture of fresh water and sediment was introduced to the basin via a constant head tank that guaranteed steady input discharge throughout each individual release. Each current passed through a momentum extraction box before entering the channel. This box was 0.5 m by 0.5 m in planform and contained several vertical screens of 5 mm wire mesh which currents passed through prior to entering the experimental channel. The momentum extraction box ensured that each flow acted as a sediment-laden plume driven by buoyancy alone. Current thickness remained constant for all 9 runs at 90 mm, while current discharge and velocity varied from flow to flow between $1.5–3.5 \times 10^{-3}$ m^3/s and 50–120 mm/s. Representative input values for the densimetric Froude number ($Fr = \bar{u}/\sqrt{[(\rho_c/\rho_a) - 1]gH}$), Reynolds number ($Re = \bar{u}H/\upsilon$), and buoyancy flux ($B_{f0} = \Delta\rho\ guhb/\rho$) for each flow are presented in Table 1, where $\bar{u}$ is depth averaged velocity, ρ_c is current density, ρ_a is the ambient fluid density, g is gravitational acceleration, H is current thickness, υ is kinematic viscosity, and b channel width. Current duration varied between 245 and 576 s.

[20] Measurements of current velocity were collected using two Sontek Acoustic Doppler Velocimeters (ADV) and one Sontek Pulse-Coherent Acoustic-Doppler Velocity Profiler (PCADP). An ADV was positioned at the channel entrance and exit throughout the experiment. These devices recorded the 3-D velocity in a 10^{-6} m^3 sampling volume located 50 mm above the channel bed at the channel centerline with a frequency of 10 Hz. Vertical profiles of velocity were collected during flow 8 at 2 distances from the channel entrance in the channel center. The PCADP measured velocity with a frequency of 0.25 Hz in sampling volumes that were 16 mm tall and varied between 0.004 to 0.006 m^2 in planform area with increasing distance from the instrument.

[21] Maps of the channel form were collected prior to flow 1, and after flows 1, 2, 3, and 8 using the first hard returns from a 1MHz ultrasonic transducer connected to a pulse/receiver box. Each bathymetric map was built from 23,184 points collected on a grid with 14.1 mm spacing in the cross-stream and downstream directions. The precision at each location is better than 0.2 mm. This resolution makes it possible to successfully determine the patterns of sediment deposition associated with individual currents by differencing successive maps of channel topography.

[22] Following the ninth current, the water level in the experimental basin was lowered, and the deposit was allowed to dry. After drying, the deposit was sampled for particle-size characterization. These samples were collected at 255 locations including sample locations centered on the left levee-crest located every 7 cm from the channel entrance. Samples were also collected from 6 cross sections oriented perpendicular to the channel centerline. Samples came from the uppermost deposit and represent deposition associated with the final currents. The sediment samples were then analyzed with a Horiba LA-300 laser-particle-size analyzer (LPSA). The LPSA uses a diode laser to accurately

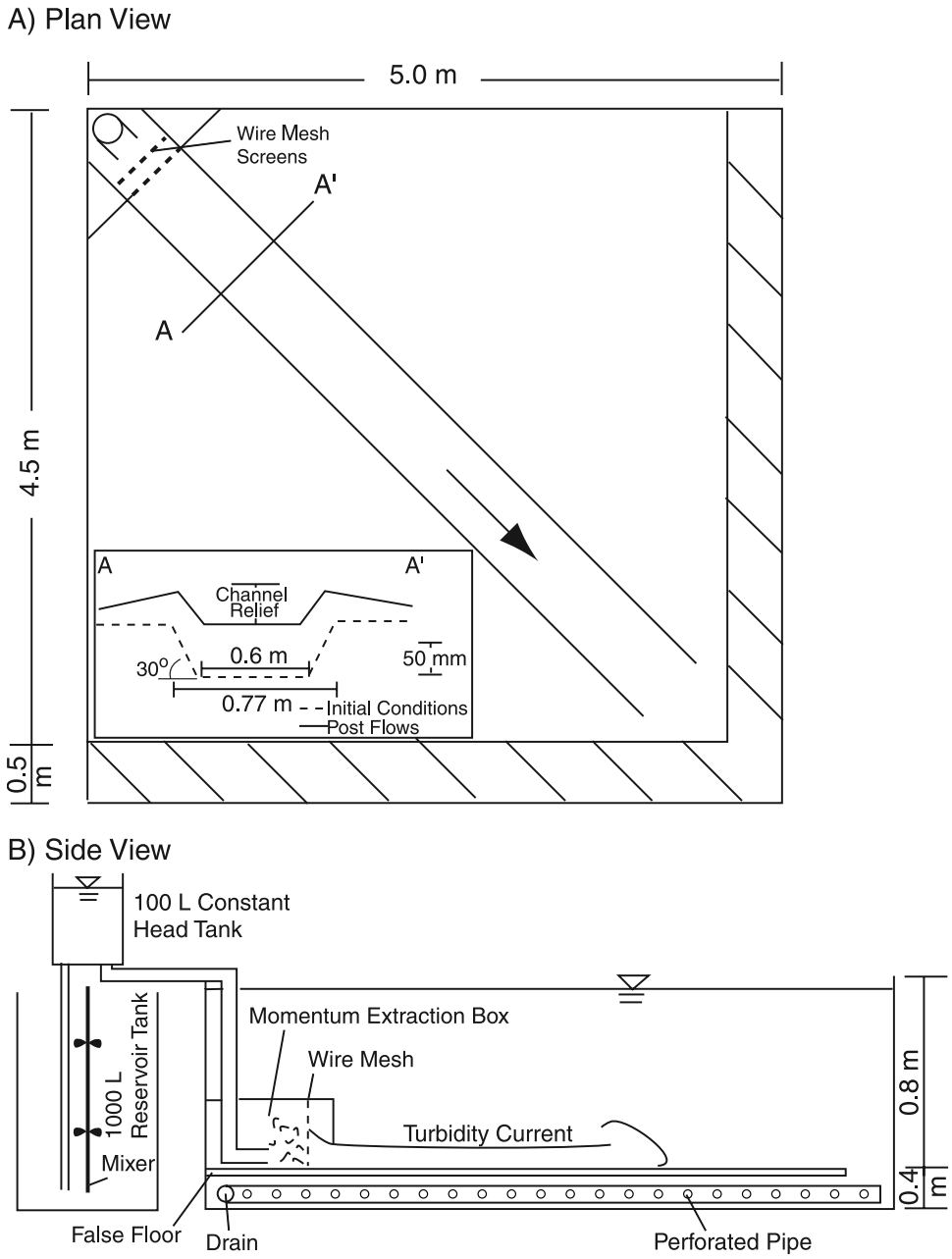

Figure 8. Schematic diagram of the experimental facility. (a) Planview of the basin and the initial channel form. Each current passed through a momentum extraction box located in the top left basin corner prior to entering the channel. Diagonal lines mark the position of a moat for collecting a current following its passage through the channel avoiding reflections off of tank walls. The insert depicts an initial and final channel cross section. (b) Side view of the facility. Each current is mixed in a reservoir tank and pumped up into a constant head tank before entering the basin.

measure a distribution of sizes from 0.001 to 0.3 mm in nominal diameter.

3.2. Scaling

[23] Our experiment was conducted at a reduced scale relative to submarine channels. A comparison of our experiment to natural environments is performed using three components: (1) a geometric scaling of the channel topography itself, (2) a dynamic scaling of flow properties for estimating equivalence between model and natural flows, and (3) a dynamic scaling of sediment-transporting conditions for roughly comparing model and natural flows. The scaling is only intended to guide how experimental results might be applied to the interpretation of natural channels. Our experiment was not designed to simulate environmental conditions associated with the construction of channels offshore Brunei.

[24] The geometric scaling for our experimental system was set at 1/1000. Maximum width, depth and length for the laboratory channel correspond to natural scales of 770 m,

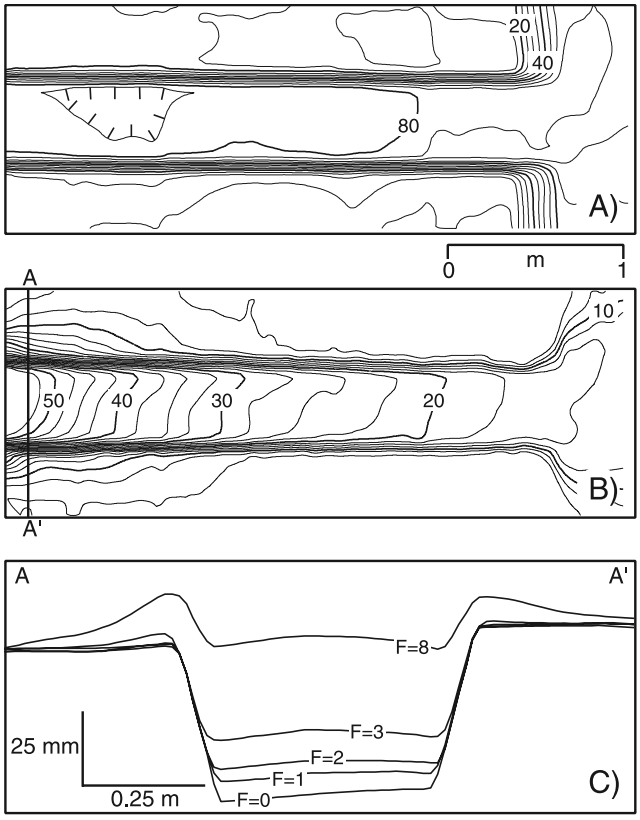

Figure 9. Maps and cross section from the experimental channel. Channel flow was from the left to the right in each map. (a) Topographic map of the initial channel form. Topography is defined as vertical distance between the bed and an overlying datum of constant elevation. Contour interval is 5 mm. (b) Map of deposit thickness from sedimentation by eight turbidity currents. This map is the difference between the initial channel form and the channel form following flow event 8. Contour interval equals 2.5 mm. (c) Evolution of channel cross sections located 0.35 m from channel entrance. Diagram displays the original channel form plus successive forms following sedimentation by flows (F) 1, 2, 3, and 8. Cross sections are oriented perpendicular to channel direction and oriented looking downstream.

50 m, and 3 km. The channel width/depth ratio measured 0.35 m from the channel entrance systematically increased from 15.4 to 42.8 through the course of the experiment. These values compare favorably with measurements from natural channels assembled by *Pirmez and Imran* [2003] and for the channels offshore Brunei.

[25] The comparison between properties of the experimental and natural or prototype flows focuses on the densimetric Froude number. An approximate dynamic similarity between the model and a natural system is ensured by setting $Fr_{(\mathrm{model})} = Fr_{(\mathrm{prototype})}$ [*Graf*, 1971]. Assuming a similar excess density for the experimental and natural currents, equality in densimetric Froude number is satisfied by prototype values for $\bar{u}$ and H of 2.2 m/s and 50 m. Equality in densimetric Froude number also constrains the duration of a comparable natural current to be 2.8 h. Reynolds numbers for the model and prototype cannot be matched. The characteristic Reynolds number for model currents was 6.4×10^3 while the characteristic value for a comparable natural current would be 3.0×10^8. Fortunately the model-current value was sufficiently large to ensure the approximate Reynolds similarity for fully turbulent gravity currents proposed by *Parsons and Garcia* [1998].

[26] Grain sizes used in the experiment can be compared to natural systems by the ratio w_s/u^* where w_s is a representative settling velocity for the particle class of interest and u^* is the shear velocity for the current. This scaling parameter was chosen because it best characterizes the degree to which particles of various sizes are suspended within the transporting current, with w_s serving as the scale value for downward particle advection and u^* being the scale value for diffusion of particles up into the interior flow by turbulent eddies. Estimates of settling velocities for experimental particles were calculated using the method of *Dietrich* [1982]. Shear velocity was estimated from a velocity profile collected at a downstream distance of 1 m positioned in the center of the channel. *Altinakar et al.* [1996] showed that the lower portions of velocity profiles for turbidity currents developing on a flat bed under approximately steady and uniform conditions exhibit a logarithmic form that can be described by

$$u(z) = \frac{u^*}{\kappa} \ln\left(\frac{z}{z_0}\right), \tag{1}$$

where $u(z)$ is the time-averaged stream-wise velocity as a function of elevation above the bed, z, κ is von Karmans' constant and is equal to 0.4, and z_0 is a roughness parameter, equal to the elevation at which the extrapolated logarithmic velocity profile goes to zero. We have estimated the characteristic shear velocity associated with the model currents, u^*_{model}, by fitting (1) to velocity data collected with the PCADP. The fit to the portion of the velocity profiles situated between and bed and the velocity maximum has a $u^*_{model} = 3.5 \times 10^{-2}$ m/s (Figure 10). A characteristic friction coefficient, C_f, for the model currents can be calculated from this estimate for u^*_{model} and the measured $\bar{u}_{model} = 5.7 \times 10^{-2}$ m/s using

$$u^* = \sqrt{C_f}\bar{u}. \tag{2}$$

The resulting $C_{f(\mathrm{model})} = 2.2 \times 10^{-2}$ is consistent with other laboratory measures of $C_{f(\mathrm{model})}$ for turbidity currents reported by *Parker et al.* [1987] and *Garcia* [1994]. A prototype shear velocity can be determined using (2) and the

Table 1. Experimental Flow Conditions

Current	U (mm/s)	Flow Duration (s)	*Fr*	*Re*	B_{f0} (m^4/s^3)
1	50	576	0.34	4.5×10^3	7.08×10^{-4}
2	60	576	0.41	5.4×10^3	8.50×10^{-4}
3	55	504	0.37	5.0×10^3	7.79×10^{-4}
4	55	504	0.37	5.0×10^3	7.79×10^{-4}
5	50	504	0.34	4.5×10^3	7.08×10^{-4}
6	70	320	0.47	6.3×10^3	9.91×10^{-4}
7	110	245	0.74	9.9×10^3	15.6×10^{-4}
8	70	320	0.47	6.3×10^3	9.91×10^{-4}
9	120	248	0.81	11×10^3	17.0×10^{-4}

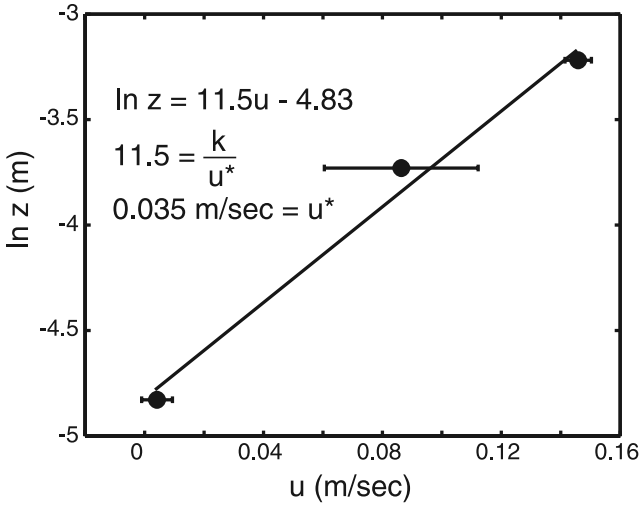

Figure 10. Estimation of model u^* obtained with best fit slope of ln z versus current velocity plot. Velocity measurements were obtained below the velocity maximum of each sample profile. Horizontal error bars are ±1 standard deviation calculated using all values for current velocity collected in each sampling volume; u^* value of the experimental flow events presented equals 0.035 m/s.

estimated values for $\bar{u}_{prototype}$ and $C_{f(\text{prototype})}$ of 2.2 m/s and 2.3×10^{-3}. We have reduced the prototype value for C_f by an order of magnitude to account for the weak dependence of bed friction coefficient with turbidity-current scale as summarized by *Parker et al.* [1987] and *Garcia* [1994]. The calculated $u^*_{prototype} = 7.0 \times 10^{-2}$ m/s. Calculated experimental values for $w_s/u^*_{(D5)}$, $w_s/u^*_{(D50)}$, and $w_s/u^*_{(D95)}$ are 7.9×10^{-5}, 1.9×10^{-2}, and 1.5×10^{-1}. All three of these values are much less than 1, the minimum value for significant suspension transport originally reported by *Bagnold* [1966]. By satisfying the equality $w_s/u^*_{(\text{model})} = w_s/u^*_{(\text{prototype})}$ we estimate that D5, D50, and D95 for the experimental flows correspond to particle sizes of 3 μm, 41 μm, 135 μm for flows at natural scale.

3.3. Experimental Results

[27] The primary goal of this experiment was to characterize the patterns of sediment deposition from turbidity currents that construct submarine levees and to connect these patterns to properties of the flow field. The nine flows that traversed our experimental channel were all highly depositional, with very little reentrainment of sediment. This resulted in deposition of sediment lamina with no internal structure and a fine-grained cap consisting of particles that did not settle out of the water column until after each current was finished. Preservation of these submillimeter-thick caps documents almost no reworking of bed material by subsequent currents. The highly depositional nature of our experimental flows makes them more analogous to channel plugging flows than channel deepening flows. As such, our experimental flows conditions are in disequilibrium with the initial channel form and suspended load. It is worth noting, however, that flows associated with channel deepening through levee construction, such as offshore Brunei, are also in disequilibrium with their guiding channel. Sediment deposition in the mapped region was small, representing a fraction of 25–30% of the total sediment released into the basin. A majority of the sediment bypassed the mapped region, exiting the channel at its downstream end. For every flow event deposition in the channel exceeded deposition on channel banks (Figures 9b and 9c), resulting in a channel that progressively lost relief over the course of the experiment. This loss of channel relief resulted in a progressive increase during the experiment in the fraction of current thickness existing above the channel overbank surface because current thickness remained constant at 0.09 m throughout the experiment. At the start of the first flow 44% of the current was situated above the overbank surface. At the end of flow 8, 81% of the current was situated above the overbank surface at a downstream location of 0.35 m from the channel entrance. No measurable decrease in current thickness or velocity was detected in the PCADP velocity profiles or overhead video.

3.3.1. Deposition on Channel Banks

[28] Deposition on the overbank surface produced levees that displayed systematic downstream trends in thickness, taper and composition. Levee taper was measured perpendicular to the channel direction and calculated using total-deposit thickness measurements, one at the levee crest and a second at a lateral position 0.2 m from the levee crest. This lateral distance equals 29% of the channel width and therefore characterizes only the most proximal section of the constructional feature. We focus on the evolution of the left-bank levee as this levee was slightly thicker than the levee on the right bank. The difference in levee thickness between the right and left bank is a result of a slight cross channel slope of approximately 0.005 m/m. Topographic data measured there defines the spatial patterns of levee deposition (Figure 11a). Near the channel entrance (x = 0.35 m), overbanking flow resulted in deposition of a 15-mm-thick levee that had a taper of 4.1×10^{-2} m/m. Both levee crest deposit thickness and taper decreased with increasing distance from the channel entrance. At 2.22 m from the channel entrance levee crest thickness and taper equaled 1.5 mm and 0.18×10^{-2} m/m. This represents a 96% decrease in levee taper between the two positions.

[29] Particle size distributions were measured along 6 transects oriented perpendicular to the channel direction. On these transects the deposit was sampled every 14 mm from 0 to 0.114 m from the levee crest (Figure 11b). Median grain size, D50, of the levee crest deposit decreased from 41 μm to 20 μm between 0.35 and 2.69 m from the channel entrance. The change in D50 with lateral distance from the channel also systematically decreased. At 0.35 m from channel entrance, grain size decreased at 2.9×10^{-2} μm/mm. At 2.69 m from the channel entrance the lateral decrease in median grain size for the levee deposit was 2.2×10^{-2} μm/mm. This represents a 24% decrease in the lateral fining of levee deposits between 0.35 and 2.69 m from the channel entrance, a much smaller percentage decrease than was measured for levee taper.

3.3.2. Current Properties

[30] To quantify the influence of current properties on levee production we must first estimate profiles of stream-wise velocity and suspended sediment concentration. Stream-wise velocity profiles were collected using a Sontek PCADP situated at the channel centerline. The profiler measured the current structure of flow 8 at two downstream

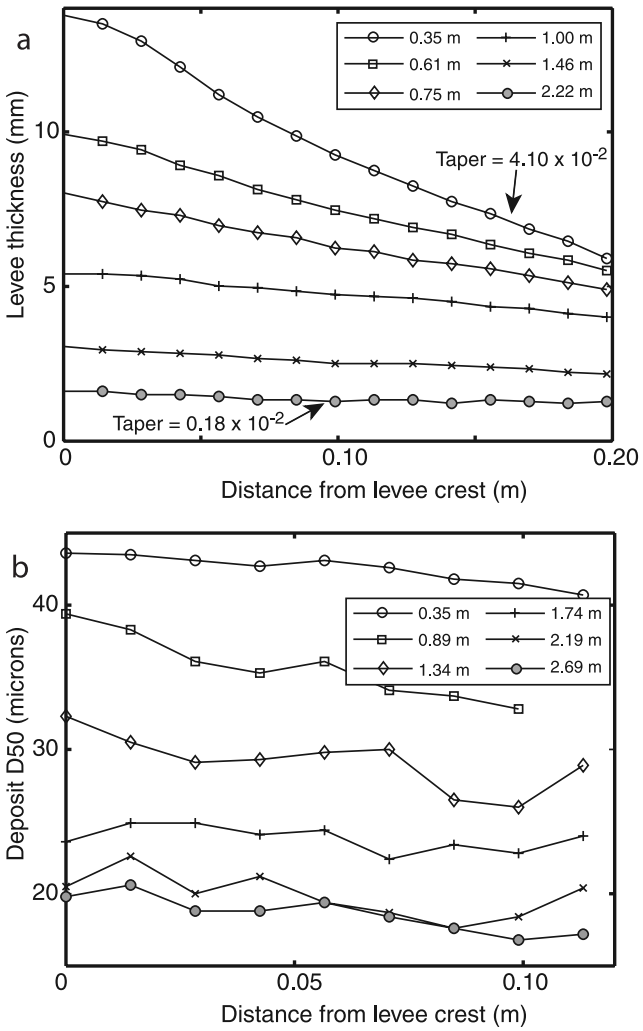

Figure 11. Cross-sectional profiles of the depositional levee at six different locations down the channel. (a) Levee thickness and taper decrease with increasing distance from the channel entrance. (b) D50 of levee deposit decrease with distance from channel entrance, but rate of D50 decrease with distance from levee crest changes negligibly with distance from channel entrance.

locations, 0.5 m and 1.5 m from the channel entrance. Mean current thickness remained constant over this distance and equaled 96 mm ± 8 mm (Figure 12). The vertical structure of the suspended-sediment concentration profile was reconstructed using properties of the levee crest deposit. This is done by assuming that mean deposition rate here was a function of the mean concentration and grain size of suspended sediment residing in the current at the levee-crest height above the channel bed. Since channel relief for flow 8 varied in the downstream direction (Figure 9) we were able to collect a set of measurements defining how the solids in this current were distributed vertically within the current. Collapsing these data collected at many points in the downstream direction onto a single, representative concentration profile requires us to assume that this profile and other current properties are slowly varying with increasing distance from the source, an assumption supported by our direct measurements of current thickness and velocity profile. Sedimentation rate for strongly depositional currents can be approximated as

$$\frac{\partial \eta}{\partial t} = w_s C_{nb}, \tag{3}$$

where C_{nb} is the near-bed concentration [*Parker et al.*, 1987]. Deposition rate on levee crests is calculated by dividing the deposit thickness on levee crests by the combined run time of the first 8 currents in our experiment. w_s is calculated for the median particle size deposited on levee crests using the method of *Dietrich* [1982]. Using this data we rearranged equation (3) to solve for C at current heights between 17 and 33 mm above the channel bed (Figure 12a). The reconstructed section of the concentration profile shows a rapid vertical decrease in concentration from 9.0×10^{-3} to 4.5×10^{-3} between 17 and 20 mm above the channel bed followed by a much less rapid decrease in concentration with increasing flow height. This rapid decrease in concentration is located at the same vertical position as the velocity maximum, confirming that there is little mixing of suspended sediment across this zone of low shear associated with the velocity maximum [*Altinakar et al.*, 1996; *Imran et al.*, 1999].

3.4. Interpretation of Laboratory Results

[31] Both levee crest deposit thickness and levee taper are plotted against the ratio of local channel relief to total current thickness, R/H, in Figure 13. This ratio describes the relative confinement of a current within the channel sidewalls at any point in the system. Values of levee-crest deposition and taper increase slowly as R/H drops from 0.49 to 0.32. Further decreases in R/H lead to rapid increases in levee-crest deposit thickness and levee taper. These observed patterns of change mimic the vertical structure of the estimated concentration profile (Figure 12). The concentration profile shows vertical stratification that is much greater than the reconstructed vertical gradient for the settling velocity profile. As the fraction of current located above the levee crest increases, the concentration of sediment located above the levee crest will also increase, resulting in enhanced sediment discharge to the overbank regions. In highly aggradational settlings, like our experiment, this will result in levee crest deposition rates that are a function of the degree of current confinement and current sediment concentration profile. We examine the connection between current confinement, sediment concentration profile, and levee taper in the following sections.

4. Comparison of Brunei and Laboratory Levees

[32] The formation and growth of levees offshore Brunei and in our laboratory experiment represent two end-member growth histories for levee evolution in aggradational settings. Levee growth offshore Brunei outpaced in-channel deposition, resulting in an increase of current confinement throughout evolution of the channels. In contrast, levee growth in our experimental channel was associated with progressive filling of a channel. As the channel filled, a larger fraction of each current was situated above the levee crest and therefore available to transition to overbank flow. We compare these two channel evolution styles by plotting

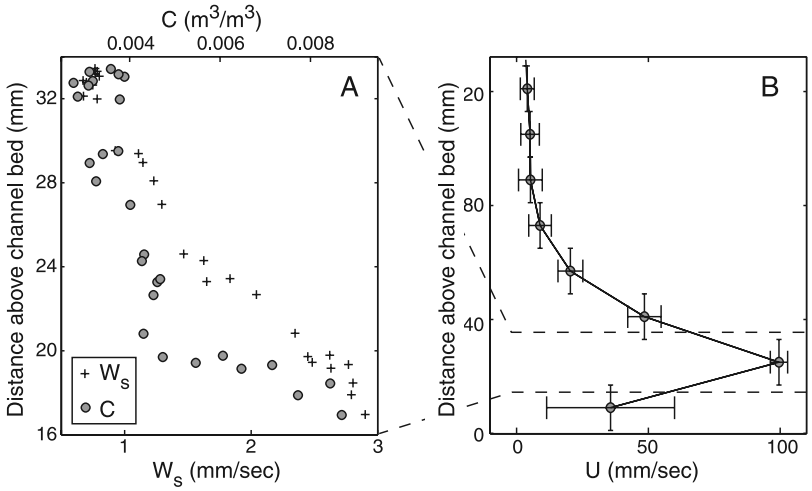

Figure 12. Vertical profiles of turbidity current properties. (a) Estimated profiles of concentration and suspended particle settling velocity calculated from deposit properties of levee crest and elevation difference between levee crest and channel centerline. (b) Profile of downstream velocity measured 0.5 m from channel entrance. Vertical error bars define the extent of each sampling volume while the horizontal error bars are ±1 standard deviation calculated using all values for current velocity collected in each sampling volume.

levee taper as a function of local channel relief (R) divided by maximum channel relief within the evolving system (R_m) (Figures 14a and 14b). We use R_m as a proxy for the vertical dimension of currents since no data on current thickness exists for offshore Brunei. The absolute magnitude of R/R_m may differ from R/H but we assume that these two parameters are highly correlated and when plotted against levee taper both ratios will produce similar trends. In the offshore Brunei system, levee taper initially increases rapidly as R/R_m grows from a very small beginning value. A rollover in this trend occurs at approximately $R/R_m = 0.04$ and levee taper increases less rapidly with further increases in R/R_m. In our laboratory experiment the growth in levee taper is initial small as R/R_m decreases from 1 to about 0.45. As R/R_m decreases further, levee taper rapidly increases. We use the similarity between the offshore Brunei and laboratory trends (Figure 14c) to guide the formulation of a simple levee growth model so that we can further explore the connections between suspended-sediment concentration profile, particle settling and advection velocities, and the degree of current confinement that lead to levee construction.

5. Levee Growth Model

[33] Inspection of submarine levees reveals that these topographic forms are primarily depositional features. In general, sediment collecting on these forms is not being substantially reworked by either the depositing or subsequent overbanking flows. Clearly this is a simplification but it provides us with a starting point for exploring submarine levee morphodynamics. We are going to assume that sediment added to levees is purely deposited from suspension fallout and that once a grain hits the bed it is transferred to the immobile substrate. Transfer to the immobile substrate precludes future mobilization as bed load or its wholesale removal via a later, net-erosional current. Under these environmental conditions we approximate the sediment transport and deposition on a levee surface using an advection-settling scheme. The vertical distribution of particle sizes and sediment concentrations are defined using the *Rouse* [1939] equation. We are aware that the structures of suspended sediment profiles described by the Rouse equation are affected by the assumption that the transporting flow has a free surface. This obviously is not the case for turbidity currents where considerable mixing and turbulence production can occur at the interface between the current and the overlying ambient fluid, seawater. In spite of this

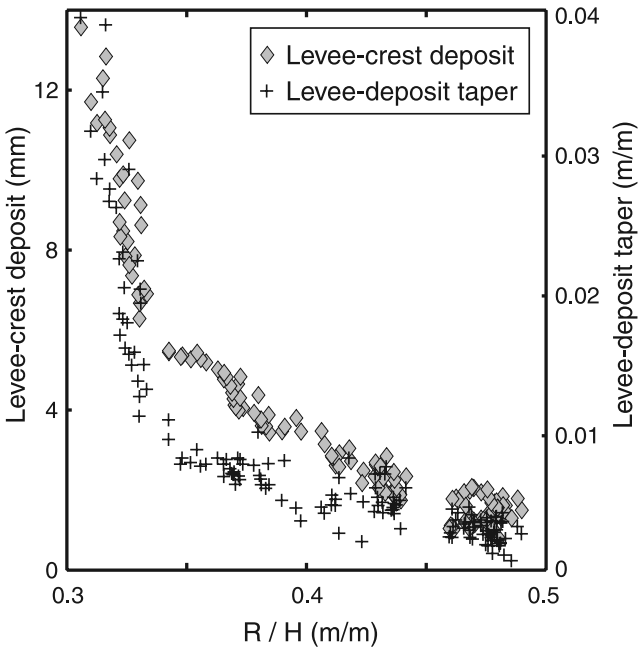

Figure 13. Comparison of change in both levee-crest deposit thickness and levee-deposit taper as a function of the ratio of local channel relief to current thickness.

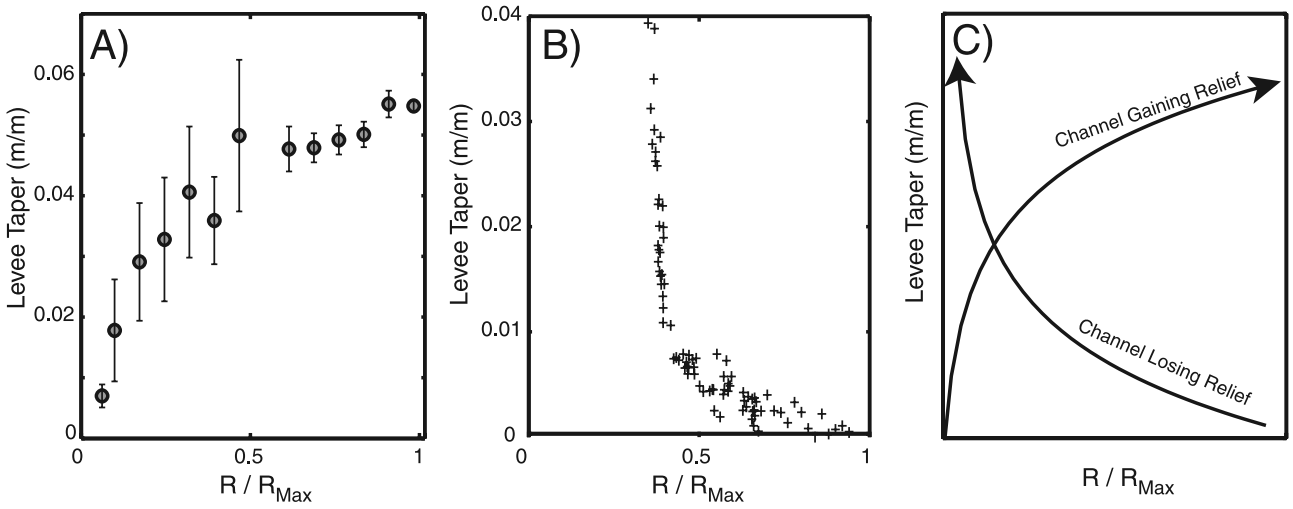

Figure 14. Evolution of levee tapers as a function of local channel relief divided by maximum channel relief for a give channel system. (a) Levee tapers measured for channel network offshore Brunei. (b) Levee tapers measured for laboratory experiment following flow 8. (c) Schematic diagram illustrating channel in levee taper for channel systems that gain relief through time and channel systems that loss relief through time.

difference, similarity between predicted and experimental profiles [*Garcia*, 1994; *Mohrig et al.*, 2005] has lead us to conclude that the Rouse equation is a useful starting point. Only that fraction of the current situated above the elevation of the levee crest is used in the advection-settling calculation. This advection-settling method results in the conservation of all sediment mass advected laterally from the channelized turbidity current via deposition and growth of levees. We envision currents with a given H, U_x, C_a, and grain size distribution leading to the growth of levees from an initially flat surface. During early channel growth, sedimentation from near-bed, relatively stratified overbanking flow will lead to levee deposits that have high tapers (Figure 15a). As the channel grows owing to levee construction, tapers of individual levee deposits will decrease as only the relatively homogeneous, better-mixed portions of the interior flow are available to leave the channel and build the levee (Figure 15b). During late stages of levee growth, individual deposits will have extremely low tapers because only the very well mixed uppermost portions of currents are able to empty onto the overbank surface (Figure 15c).

[34] Advection-settling models calculate the distance a particle will travel on the basis of the velocity of the transporting fluid and w_s. The distance a particle travels is equal to

$$x = U\frac{z_i}{w_s}, \tag{4}$$

where z_i is the initial height of the particle above the local bed elevation. Advection-settling models for sediment transport are most accurate when w_s is large compared to instantaneous, upward-directed velocities associated with the turbulent flow. We assume that this condition is met for decelerating depositional currents moving across the levee and overbank surface. Several terrestrial studies [*Adams et al.*, 2004; *Asselman and Middlekoop*, 1995; *Cazanacli and Smith*, 1998; *Filgueira-Rivera et al.*, 2007] have concluded that levee form and composition are controlled by the advection and settling of particles contained in overbank flow.

[35] We track levee elevation, η, in our model along a transect that is oriented perpendicular to the dominant flow direction. Levee deposition is influenced by current height, current velocity, the distribution of suspended particle sizes, and the structure of the suspended sediment concentration profile. We calculate a suspended-sediment concentration profile for the partially channelized flow based on input values of U_x, H, C_a, and a grain size distribution defined by one or multiple particle diameters. For each particle diameter we calculate a sediment concentration profile defined by the *Rouse* [1939] equation,

$$C_z = C_a\left(\frac{H-z}{z}\left(\frac{z_a}{H-z_a}\right)^p\right), \tag{5}$$

where C_a is a reference concentration at a given elevation, z_a, and p is the Rouse number:

$$p = \frac{w_s}{ku^*}, \tag{6}$$

where k is von Karman's constant (0.4), and u^* is the current shear velocity. u^* is calculated using equation (2), and values of $C_f = 3 \times 10^{-3}$ and $z_a = 0.8$ m. The C_f value utilized in our model represents a coefficient of friction for field-scale flows estimated by *Garcia* [1994]. Model z_a value represents an elevation associated with possible field-scale roughness elements. Deposition rate is calculated at each model node by summing of the deposition rates for each particle size included in the model,

$$\frac{\partial \eta}{dt} = \sum_i w_{si} C_{nbi}, \tag{7}$$

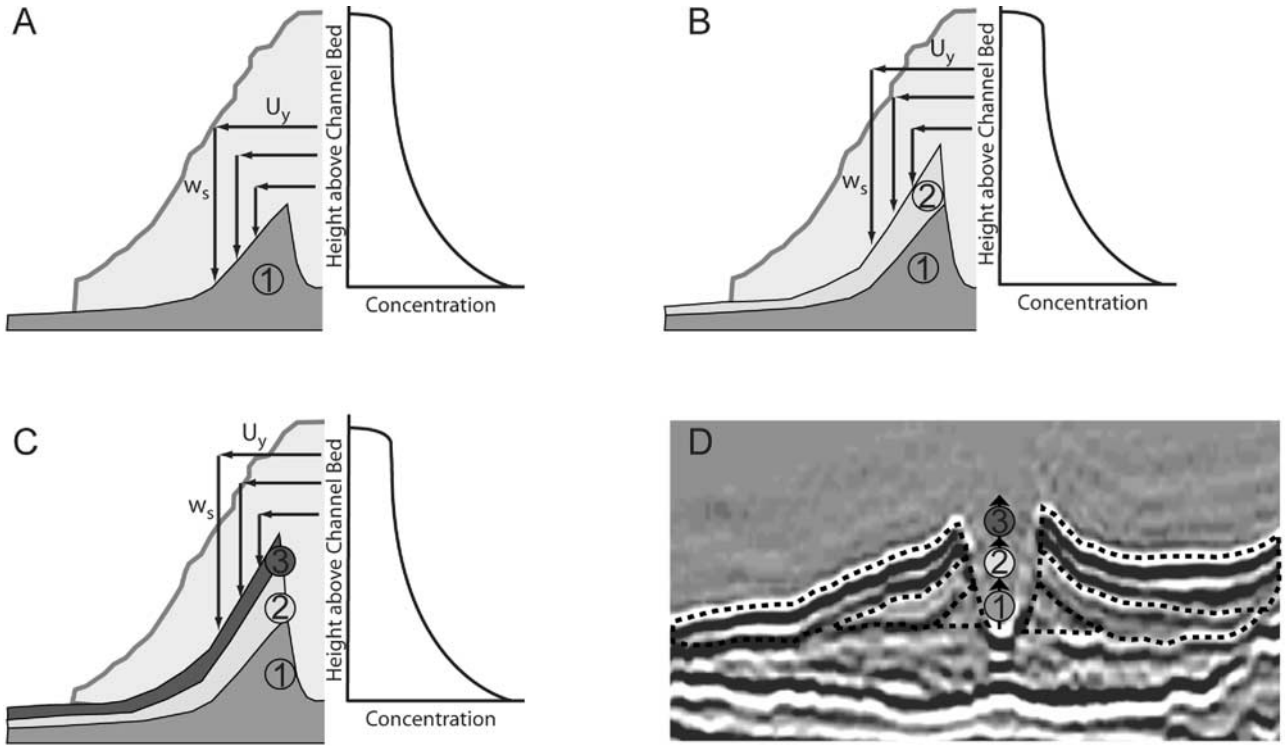

Figure 15. Schematic diagrams illustrating levee morphology evolution under aggradational conditions for bypass turbidity currents. (a) Initial channel formation and growth is associated with rapid increases in bulk levee taper as heavily stratified portion of suspended sediment concentration profile is able to exit channel. (b) As channel relief increases owing to levee deposition, lower stratified section of concentration profile progressively becomes more confined to channel, resulting in decrease in taper of individual turbidite deposits. (c) As channel relief approaches current height, only fine-grained well-mixed upper portion of turbidity current is able to spread onto overbank surface. This results in levee deposits with low tapers. (d) Seismic cross section oriented perpendicular to axis of channel B offshore Brunei. Seismic stratigraphy is similar to progression suggested in Figures 15a–15c.

where w_{si} and C_{nbi} represent the settling velocity and near bed concentration of each class i of particle diameter. C_{nb} at levee position x for each model time step is equal to

$$C_{nbx} = C_a\left(\frac{H - z_x}{z_x}\left(\frac{z_a}{H - z_a}\right)^p\right), \tag{8}$$

where z_x is the vertical position in the current contributing suspended sediment to the levee surface at distance x from the levee crest. The value of z_x is calculated using the following advection-settling expression:

$$z_x = w_s\frac{x}{U_y} + z_{LC}, \tag{9}$$

where z_{LC} represents the height of the current confining levee crest above the bed of the channel at each time step and U_y is the velocity at which sediment is advected laterally across the levee surface. As z_{LC} increases owing to levee growth an ever increasing fraction of the suspended-sediment profile becomes confined within the channel walls and is no longer available for overbanking flow. We will begin our analysis assuming a constant value of $U_y = 0.43U_x$. This relationship has been shown by *Parsons and Garcia* [1998] to describe the lateral velocity for a purely

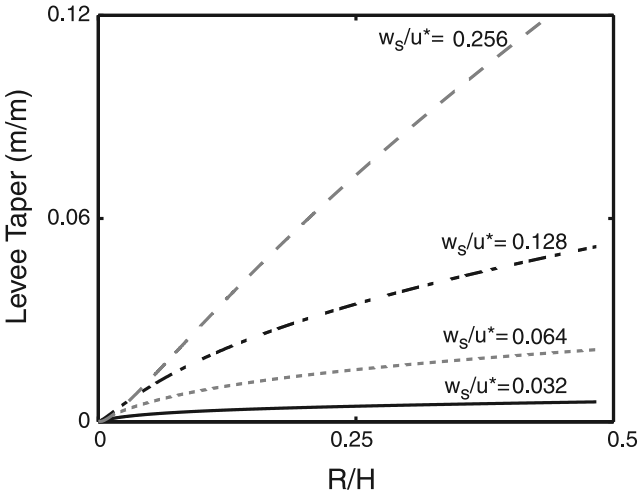

Figure 16. Model results documenting influence of sediment transport regime (w_s/u^*) on evolution of levee taper as a function of ratio between confining channel relief (R) and current thickness (H).

Table 2. Best Fit Model Parameters for Data Fit Presented in Figure 17

Parameter	Value
Ux (m/sec)	3.4
H (m)	156
C_a	0.05
Particle Size 1 (μm)	86
Particle Size 2 (μm)	93
Particle Size 3 (μm)	96
Particle Size 4 (μm)	102
Particle Size 5 (μm)	112
Particle Size 6 (μm)	153
Particle Size 7 (μm)	211
Particle Size 8 (μm)	241
Particle Size 9 (μm)	265
Particle Size 10 (μm)	291
Fr	0.57

unconfined flow in terms of the downslope directed velocity.

[36] To examine how our model performs we tracked the evolution of levee taper as a function of the ratio R/H over a range of sediment transport regimes. The results of this analysis are shown in Figure 16 for 4 values of the ratio w_s/u*. As w_s/u* increases from 0.032 to 0.256 levee taper at any value of R/H increases. In addition, as w_s/u* increases the trend of levee taper as a function of R/H becomes more linear in form.

[37] The levee growth model outlined above was used to investigate whether or not a reasonable combination of input values for U_x, H, C_a, and grain size distribution could produce a curve for levee taper growth that is similar to the trend measured from offshore Brunei (Figures 7 and 13a). We used a Monte Carlo scheme to search 100,000 combinations of the following 13 input parameters: U_x, H, C_a, and 10 particle sizes. We tracked the RMS error for each combination between our model result and the measured relationship from offshore Brunei. The RMS error was minimized by the set of parameters listed in Table 2 and visualized in Figure 17. Notice the similarity between the synthetic levee stratigraphy shown in Figure 17b and the seismically resolved stratigraphy shown in Figure 15d. The fit between the modeled levee-taper trend and the measured relationship of taper and channel relief is also quite good (Figure 17c). The model shows that the observed rollover in taper occurs at a channel relief sufficient to fully contain the highest-gradient portion of the suspended-sediment concentration profile.

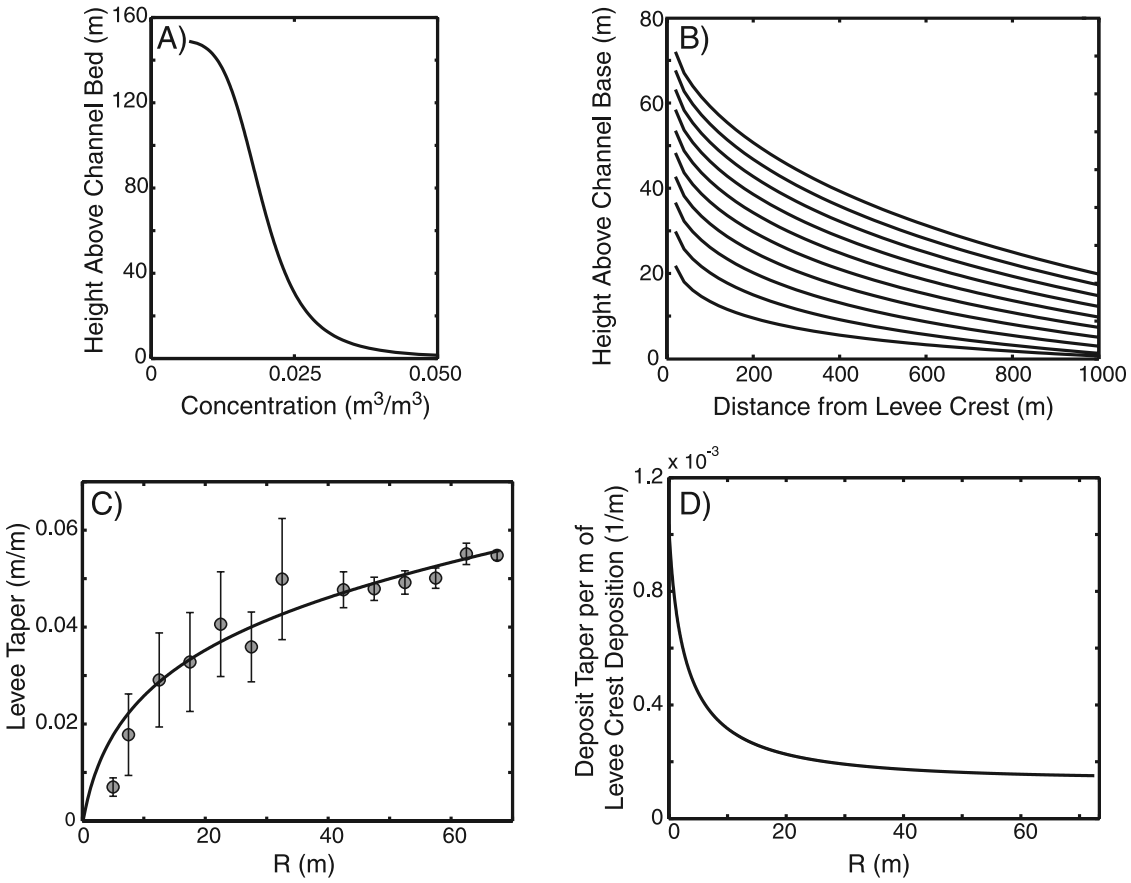

Figure 17. Results from levee growth model using input parameters detailed in Table 2. (a) Cumulative vertical suspended sediment concentration profile for the 10 particle diameters. (b) Evolution of levee topography at 10 equally spaced time steps. (c) Comparison of model and Brunei levee taper as a function channel relief. Error bars are ±1 standard deviation measured from variability in data defining deposit thickness versus distance from channel plots for each bin of channel relief. (d) Change in model deposit taper per meter of levee crest deposition as a function of channel relief.

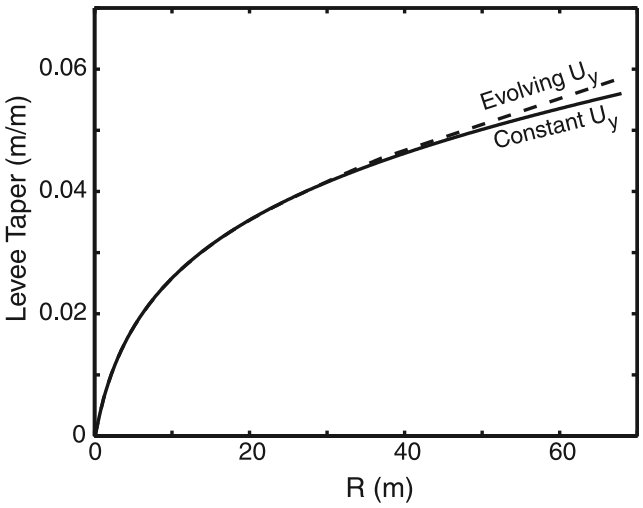

Figure 18. Comparison of levee taper growth as a function of channel relief for constant U_y model and temporally evolving U_y model.

[38] A general understanding of the relationship between current confinement and the ratio of lateral, overbank velocity to down channel, current velocity has not yet been developed. Spreading of a completely unconfined turbidity current over smooth surfaces has been studied by *Luthi* [1981], *Hauenstein and Dracos* [1984], and *Choi and Garcia* [2001]. These studies found $0.25 < U_y/U_x < 1$ for currents with widely ranging initial conditions. The evolution of U_y/U_x as a function of R/H was monitored under one set of flow conditions during an experiment presented by *Mohrig and Buttles* [2007]. They found that

$$\frac{U_y}{U_x} = 0.60e^{-3.05(R/H)}, \tag{10}$$

with $r^2 = 0.97$. We use equation (10) to compare levee growth with a varying U_y/U_x against model results for which the ratio of U_y/U_x was held constant. The best fit model parameters using the new expression for U_y/U_x are presented in Table 2. The two models produce indistinguishable results during early levee growth and only minor differences following the rollover in levee taper (Figure 18). Important for this study, though, the rollover in the two curves happens at the same value of R.

6. Discussion

6.1. Control of Concentration Profile on Levee Evolution

[39] The combination of data from offshore Brunei, our laboratory experiment and our levee growth model indicate that the shape of a suspended-sediment concentration profile most strongly influences the evolution of levee morphology. Previous studies have recognized the importance of lateral current velocity, current height, and suspended particle sizes in setting the morphology of levees [*James*, 1985; *Pizzuto*, 1987; *Skene et al.*, 2002; *Straub et al.*, 2008]. None of these studies have attempted to evaluate how levee taper changes with variation in channel relief. This study reveals that levee taper growth is primarily a function of the shape of the supralevee fraction of a current's vertical profile of sediment concentration. In our laboratory experiment we found that the relative growth in bulk levee taper was closely tied to the supralevee fraction of turbidity current thickness. The reduction in channel relief due to high in-channel deposition rates eventually elevated the high-velocity core above the channel sidewalls. This resulted in the lateral movement of some fraction of the highly stratified flow onto the overbank region (Figure 12) and the construction of levees with high tapers. Our levee growth model indicates a similar control of current confinement in the rate of levee taper growth for channels that increase their relief through time. A measurable reduction in the rate of increasing levee taper occurs after the high-concentration fraction of the flow is confined to the channel via levee and sidewall growth.

[40] We propose that channel confinement has a more important role in submarine levee evolution than in terrestrial settings. This is because submarine channels are often built by currents that can be a number of times thicker than the channels that guide them [*Hay*, 1987; *Mohrig and Buttles*, 2007; *Peakall et al.*, 2000]. For systems where current thickness is often greater than channel relief, a continuous overspill onto the overbank surface via gravitational collapse of the supralevee fraction of the flow can be expected [*Piper and Normark*, 1983]. The large dynamic range in values of R/H for submarine channels compared to rivers appears to have associated with it a greater variability in the patterns of levee sedimentation and final topographic form. This difference in the range of values for R/H is primarily a consequence of the relative density differences between turbidity currents and seawater and river flow and air.

6.2. Implications for Using Levee Stratigraphy to Estimate Current Heights

[41] The thickness of submarine channel-forming currents is difficult to measure directly owing to great water depths and infrequent flow. In addition, the depth of submarine channels bounded by levees offers only a minimum thickness for channel-building flows because turbidity currents are often much thicker than their guiding channel [*Hay*, 1987; *Mohrig and Buttles*, 2007; *Peakall et al.*, 2000]. This poses a considerable problem for modeling seascapes because current properties such as thickness are needed to accurately formulate and evaluate numerical models that simulate evolving submarine channels. Accurate estimates of paleocurrent properties are also necessary to reconstruct environmental conditions associated with ancient channel systems. *Komar* [1969] and *Pirmez and Imran* [2003] estimated turbidity current velocities in two submarine channel systems using equations that required knowledge of current height. In these two studies, the absence of a way to accurately constrain current height led the authors to equate current thickness to channel depth in order to perform their calculations of velocity. We believe results from our study point out an improved method for estimating current height from preserved levee topography.

[42] In our experiment levee taper increased as R/H decreased, owing to greater deposition on the channel bed relative to the channel margins. The rate of taper growth rapidly increased after R/H fell below $\sim$0.35 and a fraction

of the high-velocity and sediment-charged core of the currents was exposed to the suprachannel environment. *Garcia* [1994] and *Altinakar et al.* [1996] found that over a range of conditions, the high-velocity core of turbidity currents is located between 0.2 and 0.4*H*. In our experiment the location of the high-velocity core was coincident with the interval where the concentration of suspended sediment rapidly changed. Once this most stratified portion of the current was elevated above the crest lines of the channel levees, a rapid increase in levee taper occurred. Several other authors have observed a rapid change in the suspended-sediment concentration associated with the height of maximum velocity in turbidity currents [*Buckee et al.*, 2000; *Garcia and Parker*, 1993; *Parker et al.*, 1987] and have explained the connection as a result of minimal vertical mixing associated with low shear in the velocity maximum region [*Buckee et al.*, 2000]. We propose that the identification of the channel relief associated with a rapid rollover or change in growth rate of levee taper defines containment of the high-velocity and stratified core of the characteristic turbidity current by channel sidewalls. This channel relief at the rollover, R_{ro}, would therefore be $0.2H < R_{ro} < 0.4H$.

[43] For channels located offshore Brunei, a rollover in growth of levee taper occurs at a channel relief of 30 ± 5 m. Applying the surrogate for current thickness described above, we estimate the characteristic thickness of turbidity currents building the Brunei channels to be greater than 75, but less than 150 m in thickness. It is worth noting that this height is somewhat less than the estimated thickness derived using our levee growth model. We speculate that this is a result of our method for computing suspended-sediment concentration profiles. Sediment concentration profiles in our model were calculated using the Rouse equation, directly applicable to flows possessing an upper, free surface. This condition does not hold for turbidity currents and to date no consensus has been reached on how to best mathematically define the concentration profiles for these flows. Work by *Altinakar et al.* [1996] suggests that the Rouse equation does a good job of estimating turbidity current concentration profiles from the channel bed up to the elevation of the velocity maximum. Above this height they theorize that the concentration profile is modified by shear and turbulence production at the interface of turbidity currents and the overlying ambient fluid. This modification could result in reduced sediment concentrations at levels above the velocity maximum compared to those estimated using the Rouse equation. Fortunately, the rollover in levee taper occurs at a distance above the bed where the concentration profile does appear to be accurately modeled by the Rouse equation.

7. Summary

[44] In this study we use an industry grade, 3-D seismic volume to quantify the thickness of levee and regional overbank deposits that construct a tributary network of submarine channels in offshore Brunei. The initiation and growth of this channel network occurred following the release of a large mass failure. This mass failure left a 30- to 50-m-high scarp and an unchannelized slide plane. Since the release of this mass failure our study region has been a site of net deposition, allowing us to study the initiation and growth of channels from an unchannelized surface. Channel relief in this system is tied to the growth of prominent levees. These levees have an average half width of 2.1 km, a distance much less than the average distance separating channels in this network. Levee taper was measured from plots of mean deposit thickness versus distance from closest channel thalweg for channels of varying relief. We found that levee taper rapidly increased during early levee growth than transitioned to a slower taper growth rate as channel relief exceeded approximately 30 m.

[45] We monitored the growth of levees in a reduced-scale laboratory experiment. Nine turbidity currents with constant initial conditions were released into a straight channel. Preferential deposition in the channel compared to overbank surface resulted in an ever increasing fraction of the turbidity current being located above the crests of the channel-confining levees. After R/H decreased below a value of 0.35 the rate of levee taper growth rapidly increased. At these low values for R/H some fraction of the high-velocity and highly stratified core of the turbidity currents was situated above the levee crest and free to spread lateral onto the channel margins. The deposition from this highly stratified interval of the flow is the primary cause for the rapid growth in levee taper.

[46] Using our observations from the laboratory experiment we developed a levee growth model based on an advection settling scheme coupled to a sediment concentration profile defined by the Rouse equation. We found that a reasonable set of flow conditions produced a levee taper growth history that is similar to the observed trend measured from offshore Brunei. In the model a rollover to a lower growth rate for levee taper occurred following the lateral confinement of the highly stratified core flow by the thick channel-bounding levees.

[47] The observations from offshore Brunei, our laboratory experiment and our levee growth model place useful quantitative constraints on the role of current thickness, sediment-concentration profiles and confinement on the morphology of channel-bounding levees in submarine landscapes. This information can be used to estimate the thickness of channel forming turbidity currents in regions where the tapers of levees at several stages of channel growth can be measured. We propose that a measured rollover in a plot of levee taper versus channel relief is the result of progressive confinement and that $0.2H < R_{ro} < 0.4H$. The ability to estimate a characteristic thickness or height for turbidity currents associated with construction of a modern or ancient channel network will aid both forward and inverse modeling of submarine channel evolution. Further study is required to refine this estimate of current thickness from levee taper, as well as to define the dynamics of levee growth in net erosional systems and to characterize how alternating between erosional and depositional conditions affects levee morphodynamics.

Notation

b	channel width.
C_f	friction coefficient.
C_a	reference concentration.
CV	Coefficient of variation.

Fr Froude Number.
g gravitational acceleration.
H thickness of flow.
k von Karmans constant.
p Rouse number.
R channel relief.
R_m Maximum channel relief.
Re Reynolds number.
t time.
U_x down channel velocity.
U_y across channel velocity.
$\bar{u}$ depth averaged velocity.
u^* shear velocity.
w_s particle settling velocity.
z_a reference elevation.
ρ_a ambient fluid density.
ρ_c current density.
τ_b bottom shear stress.
η bed elevation.
υ kinematic viscosity.

[48] **Acknowledgments.** We thank Brunei Shell Petroleum for permission to publish seismic data from offshore Brunei Darussalam. Support for our research was provided by Shell International Exploration and Production Inc. and by the STC Program of the National Science Foundation via the National Center for Earth-Surface Dynamics under agreement EAR-0120914. Carlos Pirmez and the Shell Turbidite Research Group provided valuable help and stimulating discussions in the early stages of the project. We thank Brad Murray and Rudy Slingerland for thorough reviews of this manuscript.

References

Adams, P. N., R. L. Slingerland, and N. D. Smith (2004), Variations in natural levee morphology in anastomosed channel flood plain complexes, *Geomorphology*, *61*, 127–142, doi:10.1016/j.geomorph.2003.10.005.

Altinakar, M. S., W. H. Graf, and E. J. Hopfinger (1996), Flow structure in turbidity currents, *J. Hydraul. Res.*, *34*, 713–718.

Asselman, N. E. M., and H. Middlekoop (1995), Floodplain sedimentation: Quantities, patterns and processes, *Earth Surf. Processes Landforms*, *20*, 481–489, doi:10.1002/esp.3290200602.

Bagnold, R. A. (1966), An approach to the sediment transport problem from general physics, *U.S. Geol. Surv. Prof. Pap.*, *422-1*, 37 pp.

Brierley, G. J., R. J. Ferguson, and K. J. Woolfe (1997), What is a fluvial levee?, *Sediment. Geol.*, *114*, 1–9, doi:10.1016/S0037-0738(97)00114-0.

Buckee, C. M., B. C. Kneller, and J. Peakall (2000), Turbulence structure in steady, solute-driven gravity currents, in *Sediment Transport and Deposition by Particulate Gravity Currents*, edited by B. C. Kneller et al., *Spec. Publ. Int. Assoc. Sedimentol.*, *31*, 173–188.

Cazanacli, D., and N. D. Smith (1998), A study of morphology and texture of natural levees - Cumberland Marshes, Saskatchewan, Canada, *Geomorphology*, *25*, 43–55, doi:10.1016/S0169-555X(98)00032-4.

Choi, S.-U., and M. H. Garcia (2001), Spreading of gravity plumes on an incline, *Coastal Eng. J.*, *43*(4), 221–237, doi:10.1142/S0578563401000359.

Clark, J., and K. Pickering (1996), Architectural elements and growth patterns of submarine channels: Applications to hydrocarbon exploration, *Am. Assoc. Pet. Geol. Bull.*, *80*, 194–221.

Damuth, J. E., V. E. Koola, R. D. Flood, R. O. Kawsmann, M. C. Monteiro, J. J. C. Palma, and R. H. Belderson (1983), Distributary channel meandering and bifurcation patterns on Amazon deep-sea fan as revealed by long-range side-scan sonar (GLORIA), *Geology*, *11*, 94–98, 1983, doi:10.1130/0091-7613(1983)11<94:DCMABP>2.0.CO;2.

Demyttenaere, R., J. P. Tromp, A. Ibrahim, P. Allman-Ward, and T. Meckel (2000), Brunei deep water exploration: From sea floor images and shallow seismic analogues to depositional models in a slope-turbidite setting, paper presented at 20th Annual Research Conference, Deep-Water Reservoirs of the World, Gulf Coast Sect. Soc. of Econ. Paleontol. and Mineral. Found., Houston, Tex.

Dennielou, B., A. Huchon, C. Beaudouin, and S. Berne (2006), Vertical grain-size variability within a turbidite levee: Autocyclicity or allocyclicity? A case study from the Rhone neofan,Gulf of Lions, western Mediterranean, *Mar. Geol.*, *234*, 191–213, doi:10.1016/j.margeo.2006.09.019.

Deptuck, M. E., G. S. Steffens, M. Barton, and C. Pirmez (2003), Architecture and evolution of upper fan channel-belts on the Niger Delta slope and in the Arabian Sea, *Mar. Pet. Geol.*, *20*, 649–676, doi:10.1016/j.marpetgeo.2003.01.004.

Dietrich, W. E. (1982), Settling velocity of natural particles, *Water Resour. Res.*, *18*(6), 1615–1626, doi:10.1029/WR018i006p01615.

Felix, M., S. Sturton, and J. Peakall (2005), Combined measurements of velocity and concentration in experimental turbidity currents, *Sediment. Geol.*, *179*, 31–47, doi:10.1016/j.sedgeo.2005.04.008.

Filgueira-Rivera, M., N. D. Smith, and R. L. Slingerland (2007), Controls on natural levee development in the Columbia River, British Columbia, Canada, *Sedimentology*, *54*, 905–919.

Garcia, M. H. (1994), Depositional turbidity currents laden with poorly sorted sediment, *J. Hydraul. Eng.*, *120*, 1240–1263, doi:10.1061/(ASCE)0733-9429(1994)120:11 (1240).

Garcia, M. H., and G. Parker (1993), Experiments on the entrainment of sediment into suspension by a dense bottom current, *J. Geophys. Res.*, *98*(C3), 4793–4807, doi:10.1029/92JC02404.

Graf, W. H. (1971), *Hydraulics of Sediment Transport*, 513 pp., McGraw-Hill, New York.

Hallworth, M. A., J. C. Phillips, H. E. Huppert, and R. S. Sparks (1993), Entrainment in turbulent gravity currents, *Nature*, *362*, 829–831, doi:10.1038/362829a0.

Hauenstein, W., and T. Dracos (1984), Investigations of plunging density currents generated by inflows in lakes, *J. Hydraul. Res.*, *22*, 157–179.

Hay, A. E. (1987), Turbidity currents and submarine channel formation in Rupert Inlet, British Columbia: 2. The role of continuous and surge-type flow, *J. Geophys. Res.*, *92*(C3), 2883–2900, doi:10.1029/JC092iC03p02883.

Hiscott, R. N. (2001), Depositional sequences controlled by high rates of sediment supply, sea-level variations, and growth faulting: The Quaternary Baram Delta of northwestern Borneo, *Mar. Geol.*, *175*, 67–102, doi:10.1016/S0025-3227(01)00118-9.

Hiscott, R. N., F. R. Hall, and C. Pirmez (1997), Turbidity current overspill from Amazon Channel: Texture of the silt/sand load, paleoflow from anisotropy of magnetic susceptibility, and implications for flow processes, *Proc. Ocean Drill. Program Sci. Results*, *155*, 53–78.

Hutchison, C. S. (2004), Marginal basin evolution: The southern South China Sea, *Mar. Pet. Geol.*, *21*, 1129–1148, doi:10.1016/j.marpetgeo.2004.07.002.

Imran, J., G. Parker, and C. Pirmez (1999), A non-linear model of flow in meandering submarine and subaerial channels, *J. Fluid Mech.*, *400*, 295–331, doi:10.1017/S0022112099006515.

Ingram, G. M., T. J. Chisholm, C. J. Grant, C. A. Hedlund, P. Stuart-Smith, and J. Teasdale (2004), Deepwater North West Borneo: Hydrocarbon accumulation in an active fold and thrust belt, *Mar. Pet. Geol.*, *21*, 879–887, doi:10.1016/j.marpetgeo.2003.12.007.

James, C. S. (1985), Sediment transfer to overbank sections, *J. Hydraul. Res.*, *23*, 435–452.

Keevil, G. M., J. Peakall, J. L. Best, and K. J. Amos (2006), Flow structure in sinuous submarine channels: Velocity and turbulence structure of an experimental submarine channel, *Mar. Geol.*, *229*, 241–257, doi:10.1016/j.margeo.2006.03.010.

Khripounoff, A., A. Vangriesheim, N. Babonneau, P. Crassous, B. Dennielou, and B. Savoye (2003), Direct observations of intense turbidity current activity in the Zaire submarine valley at 4000 m water depth, *Mar. Geol.*, *194*, 151–158, doi:10.1016/S0025-3227(02)00677-1.

Komar, P. D. (1969), The channelized flow of turbidity currents with application to Monterey Deep-Sea Channel, *J. Geophys. Res.*, *74*(18), 4544–4558, doi:10.1029/JC074i018p04544.

Kostic, S., G. Parker, and J. G. Marr (2002), Role of turbidity currents in setting the forest slope of clinoforms prograding into standing fresh water, *J. Sediment. Res.*, *72*, 353–362, doi:10.1306/081501720353.

Luthi, S. (1981), Experiments on non-channelized turbidity currents, *Mar. Geol.*, *40*, M59–M68, doi:10.1016/0025-3227(81)90139-0.

Middleton, G. (1966), Experiments on density and turbidity currents I. Motion of the head, *Can. J. Earth Sci.*, *3*, 523–546.

Mohrig, D., and J. Buttles (2007), Shallow channels constructed by deep turbidity currents, *Geology*, *35*, 155–158, doi:10.1130/G22716A.1.

Mohrig, D., K. M. Straub, J. Buttles, and C. Pirmez (2005), Controls on geometry and composition of a levee built by turbidity currents in a straight laboratory channel, in *River, Coastal, and Estuarine Morphodynamics: RCEM 2005*, edited by G. Parker and M. H. Garcia, pp. 579–584, Taylor and Francis, London.

Parker, G., M. H. Garcia, Y. Fukushima, and W. Yu (1987), Experiments on turbidity currents over an erodible bed, *J. Hydraul. Res.*, *25*, 123–147.

Parsons, J. D., and M. H. Garcia (1998), Similarity of gravity current fronts, *Phys. Fluids*, *10*, 3209–3213, doi:10.1063/1.869848.

Peakall, J., B. McCaffrey, and B. Kneller (2000), A process model for the evolution, morphology, and architecture of sinuous submarine channels,

J. Sediment. Res., *70*, 434–448, doi:10.1306/2DC4091C-0E47-11D7-8643000102C1865D.

Piper, D. J. W., and W. R. Normark (1983), Turbidite depositional patterns and flow characteristics, Navy submarine fan, California Borderland, *Sedimentology*, *30*, 681–694, doi:10.1111/j.1365-3091.1983.tb00702.x.

Pirmez, C. (1994), Growth of a submarine meandering channel-levee system on the Amazon Fan, Ph.D. dissertation, 587 pp., Columbia Univ., New York.

Pirmez, C., and R. D. Flood (1995), Morphology and structure of Amazon channel, *Proc. Ocean Drill. Program Initial Rep.*, *155*, 23–45.

Pirmez, C., and J. Imran (2003), Reconstruction of turbidity currents in Amazon Channel, *Mar. Pet. Geol.*, *20*, 823–849, doi:10.1016/j.marpetgeo.2003.03.005.

Pirmez, C., R. N. Hiscott, and J. D. Kronen (1997), Sandy turbidite successions at the base of channel-levee systems of the Amazon fan revealed by FMS logs and cores: Unraveling the facies architecture of large submarine fans, *Proc. Ocean Drill. Program Sci. Results*, *155*, 7–33.

Pirmez, C., R. T. Beaubouef, S. J. Friedmann, and D. Mohrig (2000), Equilibrium profile and baselevel in submarine channels: Examples from Late Pleistocene systems and implications for the architecture of deepwater reservoirs, paper presented at 20th Annual Research Conference, Deep-Water Reservoirs of the World, Gulf Coast Sect. Soc. of Econ. Paleontol. and Mineral. Found., Houston, Tex.

Pizzuto, J. E. (1987), Sediment diffusion during overbank flows, *Sedimentology*, *34*, 301–317, doi:10.1111/j.1365-3091.1987.tb00779.x.

Posamentier, H. W. (2003), Depositional elements associated with a basin floor channel-levee system: Case study from the Gulf of Mexico, *Mar. Pet. Geol.*, *20*, 677–690, doi:10.1016/j.marpetgeo.2003.01.002.

Posamentier, H. W., and V. E. Kolla (2003), Seismic geomorphology and stratigraphy of depositional elements in deep-water settings, *J. Sediment. Res.*, *73*, 367–388, doi:10.1306/111302730367.

Prather, B. E., J. R. Booth, G. S. Steffens, and P. A. Craig (1998), Classification, lithologic calibration and stratigraphic succession of seismic facies of intraslope basins, deep-water Gulf of Mexico, *AAPG Bull.*, *92*, 707–728.

Rouse, H. (1939), Experiments on the mechanics of sediment transport, in *5th International Congress of Applied Mechanics*, edited by J. P. den Hartog and H. Peters, pp. 550–554, John Wiley, Hoboken, N. J.

Rowland, J. C., K. Lepper, W. E. Dietrich, C. J. Wilson, and R. Sheldon (2005), Tie channel sedimentation rates, oxbow formation age and channel migration rate from optically stimulated luminescences (OSL) analysis of floodplain deposits, *Earth Surf. Processes Landforms*, *30*, 1161–1179, doi:10.1002/esp.1268.

Sandal, S. T. (1996), *The Geology and Hydrocarbon Resources of Negara Brunei Darussalam*, 243 pp., Brunei Museum, Brunei Darassalam.

Skene, K. I., D. J. W. Piper, and P. S. Hill (2002), Quantitative analysis of variations in depositional sequence thickness from submarine channel levees, *Sedimentology*, *49*, 1411–1430, doi:10.1046/j.1365-3091.2002.00506.x.

Straub, K. M., D. Mohrig, B. McElroy, J. Buttles, and C. Pirmez (2008), Interactions between turbidity currents and topography in aggrading sinuous submarine channels: A laboratory study, *Geol. Soc. Am. Bull.*, *120*(3), 368–385, doi:10.1130/B25983.1.

van Rensbergen, P., C. K. Morley, D. W. Ang, T. Q. Hoan, and N. T. Lam (1999), Structural evolution of shale diapirs from reactive rise to mud volcanism: 3D seismic data from the Baram delta, offshore Brunei, Darussalam, *J. Geol. Soc.*, *156*, 633–650, doi:10.1144/gsjgs.156.3.0633.

Xu, J. P., M. A. Noble, and L. K. Rosenfeld (2004), In situ measurements of velocity structure within turbidity currents, *Geophys. Res. Lett.*, *31*, L09311, doi:10.1029/2004GL019718.

Yu, B., A. Cantelli, J. G. Marr, C. Pirmez, C. O'Byrne, and G. Parker (2006), Experiments on self-channelized subaqueous fans emplaced by turbidity currents and dilute mudflows, *J. Sediment. Res.*, *76*, 889–902, doi:10.2110/jsr.2006.069.

D. Mohrig, Department of Geological Sciences, University of Texas at Austin, Austin, TX 78712, USA. (mohrig@mail.utexas.edu)

K. M. Straub, Department of Geology and Geophysics, University of Minnesota, Minneapolis, MN 55414, USA. (kmstraub@umn.edu)